

Quantum many-body scars in the Bose-Hubbard model with a three-body constraint

Ryui Kaneko,^{1,2,3,*} Masaya Kunimi,^{4,†} and Ippei Danshita^{3,‡}

¹Waseda Research Institute for Science and Engineering, Waseda University, Shinjuku, Tokyo 169-8555, Japan

²Department of Engineering and Applied Sciences, Sophia University, Chiyoda, Tokyo 102-8554, Japan

³Department of Physics, Kindai University, Higashi-Osaka, Osaka 577-8502, Japan

⁴Department of Physics, Tokyo University of Science, Shinjuku, Tokyo 162-8601, Japan

(Dated: January 18, 2024)

We uncover the exact athermal eigenstates in the Bose-Hubbard (BH) model with a three-body constraint, motivated by the exact construction of quantum many-body scar (QMBS) states in the $S = 1$ XY model. These states are generated by applying an $SU(2)$ ladder operator consisting of a linear combination of two-particle annihilation operators to the fully occupied state. By using the improved Holstein-Primakoff expansion, we clarify that the QMBS states in the $S = 1$ XY model are equivalent to those in the constrained BH model with additional correlated hopping terms. We also find that, in the strong-coupling limit of the constrained BH model, the QMBS state exists as the lowest-energy eigenstate of the effective model in the highest-energy sector. This fact enables us to prepare the QMBS states in a certain adiabatic process and opens up the possibility of observing them in ultracold-atom experiments.

Introduction. Recent technological developments in ultracold atoms in optical lattices [1], Rydberg atoms in optical-tweezer arrays [2], trapped-ion systems [3], and superconducting qubit systems [4] allow for simulating dynamics in isolated quantum many-body systems and enable us to observe thermalization in sufficiently large systems in experiments. One of the important concepts that partly explains how isolated quantum many-body systems thermalize is the strong eigenstate thermalization hypothesis (strong ETH) [5–7]. It claims that, for all eigenstates of the quantum many-body Hamiltonian, the expectation value of a local operator coincides with that of the microcanonical ensemble, and would cause the system to thermalize after a long-time evolution [8, 9]. The strong ETH is often fulfilled in nonintegrable systems without the extensive number of conserved quantities [10, 11], but does not necessarily hold for general nonintegrable systems [12]. Indeed, such an ETH-breaking state has been observed in experiments on nonintegrable systems prepared by Rydberg atoms trapped in optical-tweezer arrays [13, 14].

The discovery of the ETH-breaking state has stimulated further studies on unconventional phenomena such as the many-body localization [15–21], the Hilbert-space fragmentation [22–26], and the quantum many-body scar (QMBS) states [26–37]. Among others, the QMBS states, in which the thermalization is extremely slow or does not occur in isolated quantum many-body systems, have gained significant attention because of their observation in a wide range of different models such as the quantum Ising and PXP models related to Rydberg-atom systems [27–29, 38–50] and optical-lattice systems [51]. Several theoretical studies have recently addressed the QMBS states in the Bose-Hubbard (BH) systems, which are commonly prepared with ultracold atoms in optical lattices, including those in the classical limit characterized by a high-dimensional chaotic phase space [52] and those emerging

due to the effects of correlated hoppings [53, 54]. However, their experimental observation is still lacking.

Although an emergent $SU(2)$ algebra that is not part of the symmetry group of the Hamiltonian helps construct the QMBS state and provides an intuitive understanding of its origin [41], to the best of our knowledge, the emergent $SU(2)$ algebra in the BH systems has not been established yet. Moreover, although the $S = 1$ XY model is commonly treated as a model for the strong-coupling limit of the BH model [55–57], the connection between the QMBS states [58, 59] [as well as the hidden $SU(2)$ algebra [60]] in the spin model and those in the bosonic one has not been thoroughly discussed. If one can systematically construct the QMBS states of BH systems in a manner similar to other spin systems, it would be much more helpful for future ultracold-atom experiments.

In this Letter, we construct the exact QMBS states in the BH model with a three-body constraint. To clarify the correspondence between the $S = 1$ XY model and the constrained BH model, we transform the spin model into the bosonic one using the improved Holstein-Primakoff expansion [61–65] and find emergent correlated hopping terms, which also possess the same QMBS states. Furthermore, by considering the strong-coupling limit of the constrained BH model, we find that the QMBS state corresponds to the lowest-energy eigenstate of the effective model in the highest-energy sector. Based on this observation, we discuss how to prepare and observe the QMBS state in ultracold-atom systems.

Scars in the constrained BH model. We consider the BH chain, which is defined as

$$\hat{H}^\infty = \hat{H}_0^\infty + \hat{H}_{\text{int}}^\infty, \quad (1)$$

$$\hat{H}_0^\infty = -J \sum_i (\hat{b}_i^\dagger \hat{b}_{i+1} + \text{H.c.}), \quad \hat{H}_{\text{int}}^\infty = \frac{U}{2} \sum_i \hat{v}_i (\hat{v}_i - 1). \quad (2)$$

Here, the operators \hat{b}_i and $\hat{v}_i = \hat{b}_i^\dagger \hat{b}_i$ correspond to the annihilation and particle number operators, respectively. We take the lattice spacing to be unity and focus on the even system size L . The strengths of the hopping and interaction are represented as J and U , respectively. The interaction U can be both attractive and repulsive. The superscript ∞ indicates that there is no

* ryuikaneko@aoni.waseda.jp

† kunimi@rs.tus.ac.jp

‡ danshita@phys.kindai.ac.jp

restriction on the maximum occupation number. We mainly choose open boundary conditions in Eq. (1) for numerical calculations although the choice of boundary conditions does not affect the presence of the QMBS states [66]

Hereafter, we focus on the model with the maximum occupation number $n_{\max} = 2$ (the occupation number at any site i is restricted to be $n_i = 0, 1$, and 2). To this end, we apply the projection $\hat{P}_{n_{\max}=2}$ on each Hamiltonian and obtain

$$\hat{H} = \hat{P}_{n_{\max}=2} \hat{H}^\infty \hat{P}_{n_{\max}=2} = \hat{H}_0 + \hat{H}_{\text{int}}, \quad (3)$$

$$\hat{H}_0 = -J \sum_i (\hat{a}_i^\dagger \hat{a}_{i+1} + \text{H.c.}), \quad \hat{H}_{\text{int}} = \frac{U}{2} \sum_i \hat{n}_i (\hat{n}_i - 1). \quad (4)$$

Here, the operators $\hat{a}_i = \hat{P}_{n_{\max}=2} \hat{b}_i \hat{P}_{n_{\max}=2}$ and $\hat{n}_i = \hat{a}_i^\dagger \hat{a}_i$ correspond to the annihilation and particle number operators after the projection, respectively. When $J \neq 0$, the BH model (for $U \neq 0$) [67] and that with the constraint $n_{\max} = 2$ (for any U) [66] are nonintegrable in general. The majority of eigenstates of these nonintegrable models should satisfy the volume-law scaling of the entanglement entropy (EE), according to the ETH. In contrast to these conventional states, we will demonstrate that the constraint model possesses the QMBS states for any interaction U .

Inspired by the previous studies on the $S = 1$ XY model [58, 59], we consider the ladder operators

$$\hat{J}^+ = \sum_i \frac{(-1)^{r_i}}{\sqrt{2}} \hat{a}_i^2, \quad \hat{J}^- = (\hat{J}^+)^\dagger \quad \text{with} \quad \hat{a} \rightarrow \begin{pmatrix} 0 & 1 & 0 \\ 0 & 0 & \sqrt{2} \\ 0 & 0 & 0 \end{pmatrix} \quad (5)$$

for the maximum occupation number $n_{\max} = 2$. Here, the matrix representation of the operator \hat{a} is obtained in the local Hilbert space spanned by $\{|0\rangle, |1\rangle, |2\rangle\}$, and r_i is the distance from the leftmost site ($r_i = i$). The operators satisfy $\hat{a}^3 = (\hat{a}^\dagger)^3 = 0$, while $\hat{a} \hat{a}^\dagger \neq \hat{a}^\dagger \hat{a} + 1$ with a three-body constraint. From these, we obtain the commutation relation $[\hat{a}_i^2, (\hat{a}_j^\dagger)^2] = (2 - 2\hat{a}_i^\dagger \hat{a}_i) \delta_{ij}$. Using this relation, we define the operator

$$\hat{J}^z = \frac{1}{2} [\hat{J}^+, \hat{J}^-] = \frac{1}{2} \sum_i (1 - \hat{a}_i^\dagger \hat{a}_i). \quad (6)$$

The operators \hat{J}^\pm and \hat{J}^z obey an SU(2) algebra ($[\hat{J}^z, \hat{J}^\pm] = \pm \hat{J}^\pm$) since $[\hat{a}_i^\dagger \hat{a}_i, \hat{a}_j^2] = -2\hat{a}_i^2 \delta_{ij}$ and $[\hat{a}_i^\dagger \hat{a}_i, (\hat{a}_j^\dagger)^2] = 2(\hat{a}_i^\dagger)^2 \delta_{ij}$. It is clear that $[\hat{J}^z, \hat{H}] = 0$ from $[\hat{J}^z, \hat{H}_0] = 0$ and $[\hat{J}^z, \hat{H}_{\text{int}}] = 0$, while $[\hat{J}^\pm, \hat{H}] \neq 0$ in general. Note that the SU(2) algebra holds for $n_{\max} = 2$ by chance and breaks down for $n_{\max} > 2$ [66].

Using the properties of these ladder operators, it is easy to show that the following states,

$$|S_n\rangle \propto (\hat{J}^+)^n |\Omega\rangle, \quad |\Omega\rangle = \bigotimes_i |2_i\rangle, \quad (7)$$

where $|2_i\rangle$ stands for $|n_i = 2\rangle$, correspond to the bosonic counterpart of the QMBS states found in the $S = 1$ XY model [58], satisfying $\hat{H}_0 |S_n\rangle = 0$ and $\hat{H}_{\text{int}} |S_n\rangle \propto |S_n\rangle$. It is given as

$$|S_n\rangle = \sum_{i_1 \neq \dots \neq i_n} \frac{(-1)^{r_{i_1} + \dots + r_{i_n}}}{\binom{L}{n}^{1/2}} \bigotimes_j \begin{cases} |0_j\rangle, & j \in \{i_1, \dots, i_n\}, \\ |2_j\rangle, & \text{otherwise,} \end{cases} \quad (8)$$

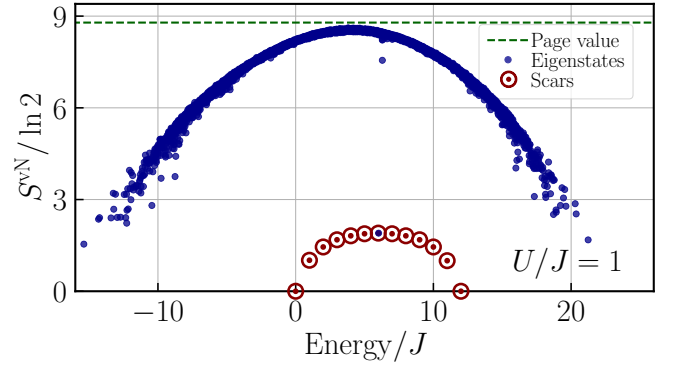


FIG. 1. EE as a function of energy. The EE of each state (a blue dot) is given in the unit of $\ln 2$, and its largest value almost saturates at the Page value [68] $S_A^{\text{Page}} = (\ln 3)L/2 - 1/2$ [58, 59] (a green dashed line). We consider the system size $L = 12$ under open boundary conditions and the interaction strength $U/J = 1$ in Eq. (3). The quantum number sector with the particle number $N = L$ (unit filling) and the even parity $\mathcal{I} = +1$ is shown. Each QMBS state (a red circle with a dot) with the particle number N has the energy $UN/2$ and the expectation values $\langle \sum_{i=1}^L \hat{n}_i \rangle = N$ and $\langle \sum_{i=1}^L \hat{n}_i^2 \rangle = 2N$. Its half-chain EE at $N = L$, corresponding to a state $|S_{n=L/2}\rangle$, becomes $S_A^{\text{vN}} \rightarrow [\ln(\pi L/8) + 1]/2$ for $L \rightarrow \infty$.

for general n . We will leave the detailed derivation for the Supplemental Material [66] and discuss in which symmetry sector the QMBS states appear. Under the space inversion symmetry operation ($\hat{\mathcal{I}}$), the boson creation operators satisfy $\hat{\mathcal{I}} \hat{a}_i^\dagger \hat{\mathcal{I}} = \hat{a}_{L+1-i}^\dagger$. The ladder operator fulfills $\hat{\mathcal{I}} \hat{J}^+ \hat{\mathcal{I}} = -\hat{J}^+$, which results in $\hat{\mathcal{I}} |S_n\rangle = (-1)^n |S_n\rangle$. This relation means that the QMBS state has even (odd) parity for even (odd) $n (= L - N/2)$ with N being the total particle number. Therefore, for even L , we should focus on the sectors with even parity $\mathcal{I} = +1$ (odd parity $\mathcal{I} = -1$) when $N = 4m$ ($N = 4m + 2$) with m being an integer.

Because the QMBS states of the BH model have exactly the same structure as those in the $S = 1$ XY model, they exhibit the same EE and the equivalent energy. The von Neumann EE is defined as $S_A^{\text{vN}} = -\text{Tr} \hat{\rho}_A \ln \hat{\rho}_A$ with $\hat{\rho}_A$ being the reduced density matrix for a region A of size L_A . When $L_A = L/2$, S_A^{vN} for the state $|S_{n=L/2}\rangle$ would be $S_A^{\text{vN}}(n = L/2) \rightarrow [\ln(\pi L/8) + 1]/2$ ($L \rightarrow \infty$) [58]. As for the energy, because the state $|S_n\rangle$ is the eigenstate of both $\hat{n}^{\text{tot}} = \sum_i \hat{n}_i$ and $\hat{d}^{\text{tot}} = \sum_i \hat{n}_i^2$, i.e., $\hat{n}^{\text{tot}} |S_n\rangle = 2(L - n) |S_n\rangle$, $\hat{d}^{\text{tot}} |S_n\rangle = 4(L - n) |S_n\rangle$, the equation $\hat{H} |S_n\rangle = (\hat{H}_0 + \hat{H}_{\text{int}}) |S_n\rangle = \frac{U}{2} N |S_n\rangle$ holds with the number of total particles $N = 2(L - n)$ ($= 0, 2, 4, \dots, 2L - 2, 2L$).

Numerical results on the corresponding EE versus the energy are presented in Fig. 1. Most of the eigenstates exhibit the volume-law scaling of EE, whereas the QMBS states show the area-law scaling (with a logarithmic correction) of EE.

Correspondence between the $S = 1$ XY model and the constrained BH model. Let us first present the transformation that we use to study the correspondence between the two models. We utilize the improved Holstein-Primakoff expansion [61–

[65] for $S = 1$ spin operators

$$\hat{S}_i^+ = \sqrt{2}\hat{b}_i + (1 - \sqrt{2})\hat{b}_i^\dagger\hat{b}_i^2 + \left(\frac{1}{\sqrt{2}} - 1\right)(\hat{b}_i^\dagger)^2\hat{b}_i^3, \quad (9)$$

with \hat{b}_i being the boson annihilation operator before the Hilbert space truncation. The advantage over the conventional Holstein-Primakoff expansion is that the Hilbert space on which the operator acts splits into the physical ($n_i = 0, 1, \dots, n_{\max} = 2$) and unphysical ($n_i = n_{\max} + 1, n_{\max} + 2, \dots$) spaces [66]. Therefore, as long as the operator acts on the state in the physical subspace, the generated states remain physical. The transformation within the physical subspace does not change the spectra of eigenenergies. Consequently, the bosonic operators with the truncated Hilbert space $n_{\max} = 2$ (namely, $\hat{a}_i = \hat{P}_{n_{\max}=2}\hat{b}_i\hat{P}_{n_{\max}=2}$) can be mapped exactly to $S = 1$ spin operators. Then, the spin ladder operator $\hat{K}^+ = \frac{1}{2}\sum_i(-1)^{r_i}(\hat{S}_i^+)^2$, which is used for constructing the QMBS states in the $S = 1$ XY model [58, 59], is evaluated as

$$\hat{K}^+ = \frac{1}{2}\sum_i(-1)^{r_i}\left[\sqrt{2}\hat{b}_i^2 - \sqrt{2}\hat{b}_i^\dagger\hat{b}_i^3 + \frac{1}{\sqrt{2}}(\hat{b}_i^\dagger)^2\hat{b}_i^4 + (5 - 3\sqrt{2})(\hat{b}_i^\dagger)^3\hat{b}_i^5 + \left(\frac{3}{2} - \sqrt{2}\right)(\hat{b}_i^\dagger)^4\hat{b}_i^6\right]. \quad (10)$$

We immediately see $\hat{K}^+ \rightarrow \hat{J}^+$ with a three-body constraint ($\hat{a}_i^3 = \hat{P}_{n_{\max}=2}\hat{b}_i^3\hat{P}_{n_{\max}=2} = 0$), indicating the QMBS states in both systems are equivalent.

We then transform the term $\hat{H}_0^{XY} = J_{xy}\sum_i(\hat{S}_i^x\hat{S}_{i+1}^x + \hat{S}_i^y\hat{S}_{i+1}^y)$ in the $S = 1$ XY system into the bosonic one. Expanding it by the bosonic operator \hat{b}_i , we get correlated hopping terms in addition to the conventional boson hopping term:

$$\begin{aligned} \hat{H}_0^{XY} &= J_{xy}\sum_i(\hat{b}_i\hat{b}_{i+1}^\dagger + \text{H.c.}) \\ &+ \left(\frac{1}{\sqrt{2}} - 1\right)J_{xy}\sum_i(\hat{b}_i\hat{b}_{i+1}^\dagger\hat{v}_{i+1} + \hat{b}_{i+1}\hat{b}_i^\dagger\hat{v}_i + \text{H.c.}) \\ &+ \left(\frac{3}{2} - \sqrt{2}\right)J_{xy}\sum_i(\hat{v}_i\hat{b}_i\hat{b}_{i+1}^\dagger\hat{v}_{i+1} + \text{H.c.}). \end{aligned} \quad (11)$$

Here, we drop unphysical higher-order terms, which correspond to those containing \hat{b}_i^3 at the rightmost end. Correlated hoppings are known to play a crucial role in stabilizing the QMBS states [53, 54, 69]. By utilizing the improved Holstein-Primakoff expansion, we successfully show that the correlated hopping terms in our model also possess the same QMBS as in the original constrained BH model [66].

Scars in the strong-coupling limit. Let us discuss how the QMBS states behave in the strong-coupling limit, which will be useful for experimental realization as we will explain later. We consider the strong-coupling limit of the BH model on an open chain with a three-body constraint at unit filling: $\hat{H} = -J\sum_{i=1}^{L-1}(\hat{a}_i^\dagger\hat{a}_{i+1} + \hat{a}_{i+1}^\dagger\hat{a}_i) + \sum_{i=1}^L\Omega_i\hat{n}_i + \frac{U}{2}\sum_{i=1}^L\hat{n}_i(\hat{n}_i - 1)$. Here, Ω_i is the external potential, which is often chosen to be a parabolic one in experiments, and the local Hilbert space is spanned by $\{|0\rangle, |1\rangle, |2\rangle\}$. We derive the effective model in the strong U/J limit for the Hilbert subspace satisfying

$\sum_i n_i = N$ (unit filling) and $n_i = 0$ or 2 using the Schrieffer-Wolff transformation [70, 71]:

$$\begin{aligned} \hat{H}_{\text{eff}} &= \frac{1}{2}LU + \sum_{i=1}^L\Omega_i + \frac{1}{2}\sum_{i=1}^{L-1}\tilde{J}_{i,i+1} + \sum_{i=1}^L\tilde{h}_i\hat{T}_i^z \\ &+ 2\sum_{i=1}^{L-1}\tilde{J}_{i,i+1}(\hat{T}_i^x\hat{T}_{i+1}^x + \hat{T}_i^y\hat{T}_{i+1}^y - \hat{T}_i^z\hat{T}_{i+1}^z). \end{aligned} \quad (12)$$

Here, we define

$$\tilde{h}_i := 2\Omega_i - (J_{i,i+1}^+ - J_{i,i+1}^-) + (J_{i-1,i}^+ - J_{i-1,i}^-), \quad (13)$$

$$\tilde{J}_{i,i+1} := J_{i,i+1}^+ + J_{i,i+1}^- = \frac{2J^2U}{U^2 - (\Omega_{i+1} - \Omega_i)^2}, \quad (14)$$

$$J_{i,i+1}^\pm := \begin{cases} \frac{J^2}{U \pm (\Omega_{i+1} - \Omega_i)}, & i = 1, 2, \dots, L-1, \\ 0, & i = 0, L. \end{cases} \quad (15)$$

The operators \hat{T}^α ($\alpha = x, y, z$) are the $S = 1/2$ spin operators that act on the space spanned by $\{|0\rangle, |2\rangle\}$, and satisfy $\hat{T}^z = (|2\rangle\langle 2| - |0\rangle\langle 0|)/2$ and $\hat{T}^+ = |2\rangle\langle 0|$. Note that a similar effective model was derived previously [72–75] although they are different from the present one which prohibits the hopping process containing $n_i > 2$.

After performing a spin rotation around the z axis by π radians for even sites, the effective model in Eq. (12) transforms into the ferromagnetic Heisenberg model in the absence of the external potential ($\Omega_i = 0$). The ground state after the transformation is a trivial ferromagnetic state, which includes a state $|\psi_{\text{GS}}^{\text{FM}}\rangle \propto \hat{P}_{\text{UF}} \otimes_{j=1}^L \frac{|0_j\rangle + |2_j\rangle}{\sqrt{2}}$ at unit filling. Here, \hat{P}_{UF} is a projection onto the space at unit filling ($\sum_i n_i = L$). Then, the corresponding ground state of the original effective model in Eq. (12) becomes $|\psi_{\text{GS}}^{\text{AF}}\rangle \propto \hat{P}_{\text{UF}} \otimes_{j=1}^L \frac{|0_j\rangle - (-1)^j|2_j\rangle}{\sqrt{2}}$, which is equivalent to $|S_{L/2}\rangle$ in Eq. (8). Therefore, the exact ground state of the effective model in the strong-coupling limit is embedded in the spectra of eigenstates of the constrained BH model. Note that the effect of small external potential is found to be negligible [66].

Next, let us consider how the QMBS state behaves in the case of $U/J < \infty$. For $U \gg J$, the energy spectrum is divided into well separated bands, and the eigenstates belonging to each band nearly preserve the number of sites at which the particle number takes the values $n_i = 0$, $n_i = 1$, and $n_i = 2$. In the case of unit filling with a three-body constraint, the highest-energy band (consisting of $L/2$ sites with $n_i = 0$ and $L/2$ sites with $n_i = 2$ only) and the second highest-energy band (consisting of $L/2 - 1$ sites with $n_i = 0$, $L/2 - 1$ sites with $n_i = 2$, and remaining 2 sites with $n_i = 1$) are well separated energetically (see Fig. 2). Because the QMBS state is the exact eigenstate of the constrained BH model for any U , we can always find the QMBS eigenstate in the band consisting of only $n_i = 0$ and $n_i = 2$ sites. Remarkably, we have found that the QMBS state corresponds to the lowest-energy eigenstate in this subspace (the highest-energy band) not only at the strong-coupling limit $J/U = 0$ but also for $J/U \leq 0.1$, using the exact diagonalization method for $L \leq 12$ [66].

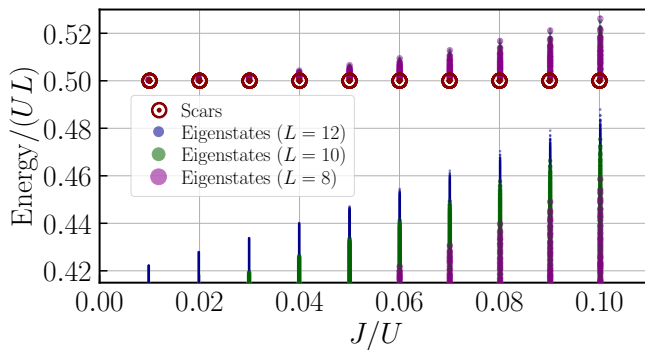


FIG. 2. Energy spectra as a function of the interaction strength at unit filling. We consider the Hamiltonian in Eq. (3) without the external potential under open boundary conditions, the system size $L = 8, 10$, and 12 , and the interaction strength $J/U = 0.01, 0.02, \dots, 0.1$. The quantum number sector with the particle number $N = L$ and the parity $\mathcal{I} = (-1)^{\text{mod}(L,4)/2}$ for $L = 8, 10$, and 12 is given by largest purple, middle green, and smallest blue dots, respectively. Each QMBS state (a red circle with a dot) with the particle number $N (= L)$ has the energy $UN/2$. The effective subspace exhibiting the highest energy ($\approx UL/2$) and that exhibiting the second highest one ($\approx UL/2 - U$) are well separated energetically for $U \gg J$. The QMBS state is found to become the lowest-energy eigenstate in the former subspace for sufficiently strong interaction.

Preparing scars in ultracold-atom experiments. For a wide parameter region of $U \gg J$, the QMBS state is found to become the lowest-energy eigenstate in the highest-energy band, where the particle number takes only the values 0 and 2 . Therefore, it would be possible to achieve QMBS states in the BH model with a three-body constraint in the following manner: (i) Prepare the $202020\dots$ -type charge-density wave (CDW) state with a choice of $\Omega_i = \text{const} \times (-1)^i$ to join in the effective $n_i = 0, 2$ subspace [76]. (ii) Make the external potential nearly uniform ($\Omega_i \approx \text{const}$) by adiabatically changing it while keeping U/J sufficiently strong. The quantum adiabatic theorem ensures that the final state approaches the lowest-energy eigenstate (equivalent to $|S_{L/2}\rangle$) in the $n_i = 0, 2$ subspace. (iii) Subsequently reduce the potential depth so that the strength of the interaction becomes comparable to the magnitude of hopping. Note that the ETH breaking may be caused by the fragmentation [75] and the QMBS states for $U \gg J$. To purely observe the effect of the QMBS states, it is desirable to prepare the system with smaller U .

Concerning the three-body constraint, strong three-body losses of atoms in optical lattices prohibit more than two particles from occupying a single site because of the continuous quantum Zeno effect, resulting in the Bose-Hubbard model with $n_{\text{max}} = 2$ [76, 77]. To allow control over the ratio of the three-body-loss term to the two-body interaction term, one can use a broad Feshbach resonance [78–80]. This procedure enables us to realize the much stronger three-body-loss term than the interaction and hopping terms, while keeping peri-

odic potentials shallow so that the interaction is not so strong. Because our QMBS states in the constrained BH model can be realized for both attractive and repulsive interactions, they would be detected in ultracold atoms with three-body losses in optical lattices.

In such QMBS states with a fixed particle number, most of the physical quantities (such as single-particle correlations [81], density-density correlations [82], and the Rényi EE [83, 84]) exhibit almost no time dependence, which would be observed after a sudden quench in experiments. The logarithmic size dependence of the EE growth would also provide a smoking gun for the existence of the QMBS states.

Conclusions. Motivated by the exact construction of the QMBS states in the $S = 1$ XY model, we have provided the equivalent athermal states in the BH model with a three-body constraint. To get insight into the mechanism of realizing the QMBS states in the bosonic system, we transform the spin model into the bosonic model using the improved Holstein-Primakoff transformation [61–65] that does not mix the physical and unphysical Hilbert spaces and consequently does not change the exact energy spectra. The bosonic model obtained after the transformation is similar to the conventional BH model, but with the additional correlated hopping terms, which also possess the same QMBS states. Based on the fact that the QMBS state corresponds to the lowest-energy eigenstate of the effective model for the strong-coupling limit with the highest-energy sector, we propose the realization of the QMBS states in ultracold-atom systems. Moreover, such a local effective Hamiltonian, which also possesses the QMBS states as its eigenstates, would deepen our understanding of the scar phenomena.

Our findings will stimulate further research on the QMBS states in general BH models without any constraints, which would be realized more easily in experiments of ultracold atoms in optical lattices. The construction of the QMBS states in the general spin S system has been discussed recently [85, 86], and it could be extended to the BH model by utilizing the improved Holstein-Primakoff transformation [61–65]. These QMBS states do not have to be generated according to the conventional $SU(2)$ algebra [85, 86]. This topic will be left for a subject of future study.

ACKNOWLEDGMENTS

The authors acknowledge fruitful discussions with Shimpei Goto, Daichi Kagamihara, Hosho Katsura, Mathias Mikkelsen, and Daisuke Yamamoto. This work was financially supported by JSPS KAKENHI (Grants No. JP18H05228, No. JP20K14389, No. JP21H01014, No. JP21K13855, and No. JP22H05268), by MEXT Q-LEAP (Grant No. JPMXS0118069021), and by JST FOREST (Grant No. JPMJFR202T). The numerical computations were performed on computers at the Supercomputer Center, the Institute for Solid State Physics, the University of Tokyo.

- [1] S. Trotzky, Y.-A. Chen, A. Flesch, I. P. McCulloch, U. Schollwöck, J. Eisert, and I. Bloch, *Nat. Phys.* **8**, 325 (2012).
- [2] A. Browaeys and T. Lahaye, *Nat. Phys.* **16**, 132 (2020).
- [3] R. Blatt and C. F. Roos, *Nat. Phys.* **8**, 277 (2012).
- [4] C. Neill, P. Roushan, M. Fang, Y. Chen, M. Kolodrubetz, Z. Chen, A. Megrant, R. Barends, B. Campbell, B. Chiaro, A. Dunsworth, E. Jeffrey, J. Kelly, J. Mutus, P. J. J. O'Malley, C. Quintana, D. Sank, A. Vainsencher, J. Wenner, T. C. White, A. Polkovnikov, and J. M. Martinis, *Nat. Phys.* **12**, 1037 (2016).
- [5] J. M. Deutsch, *Phys. Rev. A* **43**, 2046 (1991).
- [6] M. Srednicki, *Phys. Rev. E* **50**, 888 (1994).
- [7] M. Rigol, V. Dunjko, and M. Olshanii, *Nature* **452**, 854 (2008).
- [8] T. Mori, T. N. Ikeda, E. Kaminishi, and M. Ueda, *J. Phys. B: At. Mol. Opt. Phys.* **51**, 112001 (2018).
- [9] L. D'Alessio, Y. Kafri, A. Polkovnikov, and M. Rigol, *Adv. Phys.* **65**, 239 (2016).
- [10] W. Beugeling, R. Moessner, and M. Haque, *Phys. Rev. E* **89**, 042112 (2014).
- [11] H. Kim, T. N. Ikeda, and D. A. Huse, *Phys. Rev. E* **90**, 052105 (2014).
- [12] N. Shiraishi and T. Mori, *Phys. Rev. Lett.* **119**, 030601 (2017).
- [13] H. Bernien, S. Schwartz, A. Keesling, H. Levine, A. Omran, H. Pichler, S. Choi, A. S. Zibrov, M. Endres, M. Greiner, V. Vuletić, and M. D. Lukin, *Nature* **551**, 579 (2017).
- [14] D. Bluvstein, A. Omran, H. Levine, A. Keesling, G. Semeghini, S. Ebadi, T. T. Wang, A. A. Michailidis, N. Maskara, W. W. Ho, S. Choi, M. Serbyn, M. Greiner, V. Vuletic, and M. D. Lukin, *Science* **371**, 1355 (2021).
- [15] R. Nandkishore and D. A. Huse, *Annu. Rev. Condens. Matter Phys.* **6**, 15 (2015).
- [16] J.-y. Choi, S. Hild, J. Zeiher, P. Schauß, A. Rubio-Abadal, T. Yefsah, V. Khemani, D. A. Huse, I. Bloch, and C. Gross, *Science* **352**, 1547 (2016).
- [17] M. Yan, H.-Y. Hui, M. Rigol, and V. W. Scarola, *Phys. Rev. Lett.* **119**, 073002 (2017).
- [18] M. Yan, H.-Y. Hui, and V. W. Scarola, *Phys. Rev. A* **95**, 053624 (2017).
- [19] F. Alet and N. Laflorencie, *Comptes Rendus Physique* **19**, 498 (2018).
- [20] D. A. Abanin, E. Altman, I. Bloch, and M. Serbyn, *Rev. Mod. Phys.* **91**, 021001 (2019).
- [21] A. Mokhtari-Jazi, M. R. Fitzpatrick, and M. P. Kennett, *Nucl. Phys. B* **997**, 116386 (2023).
- [22] P. Sala, T. Rakovszky, R. Verresen, M. Knap, and F. Pollmann, *Phys. Rev. X* **10**, 011047 (2020).
- [23] V. Khemani, M. Hermele, and R. Nandkishore, *Phys. Rev. B* **101**, 174204 (2020).
- [24] Z.-C. Yang, F. Liu, A. V. Gorshkov, and T. Iadecola, *Phys. Rev. Lett.* **124**, 207602 (2020).
- [25] S. Moudgalya and O. I. Motrunich, *Phys. Rev. X* **12**, 011050 (2022).
- [26] S. Moudgalya, B. A. Bernevig, and N. Regnault, *Rep. Prog. Phys.* **85**, 086501 (2022).
- [27] C. J. Turner, A. A. Michailidis, D. A. Abanin, M. Serbyn, and Z. Papić, *Nat. Phys.* **14**, 745 (2018).
- [28] C. J. Turner, A. A. Michailidis, D. A. Abanin, M. Serbyn, and Z. Papić, *Phys. Rev. B* **98**, 155134 (2018).
- [29] A. J. A. James, R. M. Konik, and N. J. Robinson, *Phys. Rev. Lett.* **122**, 130603 (2019).
- [30] N. Shibata, N. Yoshioka, and H. Katsura, *Phys. Rev. Lett.* **124**, 180604 (2020).
- [31] D. K. Mark and O. I. Motrunich, *Phys. Rev. B* **102**, 075132 (2020).
- [32] Y. Kuno, T. Mizoguchi, and Y. Hatsugai, *Phys. Rev. B* **102**, 241115(R) (2020).
- [33] Z. Papić, Weak ergodicity breaking through the lens of quantum entanglement, in *Entanglement in Spin Chains: From Theory to Quantum Technology Applications*, edited by A. Bayat, S. Bose, and H. Johannesson (Springer, Cham, 2022) pp. 341–395.
- [34] M. Serbyn, D. A. Abanin, and Z. Papić, *Nat. Phys.* **17**, 675 (2021).
- [35] H. Yoshida and H. Katsura, *Phys. Rev. B* **105**, 024520 (2022).
- [36] A. Chandran, T. Iadecola, V. Khemani, and R. Moessner, *Annual Review of Condensed Matter Physics* **14**, 443 (2023).
- [37] K. Sanada, Y. Miao, and H. Katsura, *Phys. Rev. B* **108**, 155102 (2023).
- [38] N. Shiraishi, *J. Stat. Mech.* **2019**, 083103 (2019).
- [39] K. Bull, I. Martin, and Z. Papić, *Phys. Rev. Lett.* **123**, 030601 (2019).
- [40] C.-J. Lin and O. I. Motrunich, *Phys. Rev. Lett.* **122**, 173401 (2019).
- [41] S. Choi, C. J. Turner, H. Pichler, W. W. Ho, A. A. Michailidis, Z. Papić, M. Serbyn, M. D. Lukin, and D. A. Abanin, *Phys. Rev. Lett.* **122**, 220603 (2019).
- [42] W. W. Ho, S. Choi, H. Pichler, and M. D. Lukin, *Phys. Rev. Lett.* **122**, 040603 (2019).
- [43] B. Mukherjee, S. Nandy, A. Sen, D. Sen, and K. Sengupta, *Phys. Rev. B* **101**, 245107 (2020).
- [44] C.-J. Lin, V. Calvera, and T. H. Hsieh, *Phys. Rev. B* **101**, 220304(R) (2020).
- [45] C.-J. Lin, A. Chandran, and O. I. Motrunich, *Phys. Rev. Res.* **2**, 033044 (2020).
- [46] T. Iadecola and M. Schechter, *Phys. Rev. B* **101**, 024306 (2020).
- [47] A. A. Michailidis, C. J. Turner, Z. Papić, D. A. Abanin, and M. Serbyn, *Phys. Rev. Res.* **2**, 022065(R) (2020).
- [48] S. Sugiura, T. Kuwahara, and K. Saito, *Phys. Rev. Res.* **3**, L012010 (2021).
- [49] Z. Yao, L. Pan, S. Liu, and H. Zhai, *Phys. Rev. B* **105**, 125123 (2022).
- [50] M. Kunimi, T. Tomita, H. Katsura, and Y. Kato, *arXiv:2306.05591*.
- [51] G.-X. Su, H. Sun, A. Hudomal, J.-Y. Desaulles, Z.-Y. Zhou, B. Yang, J. C. Halimeh, Z.-S. Yuan, Z. Papić, and J.-W. Pan, *Phys. Rev. Res.* **5**, 023010 (2023).
- [52] Q. Hummel, K. Richter, and P. Schlagheck, *Phys. Rev. Lett.* **130**, 250402 (2023).
- [53] H. Zhao, J. Vovrosh, F. Mintert, and J. Knolle, *Phys. Rev. Lett.* **124**, 160604 (2020).
- [54] A. Hudomal, I. Vasić, N. Regnault, and Z. Papić, *Commun. Phys.* **3**, 99 (2020).
- [55] E. Altman and A. Auerbach, *Phys. Rev. Lett.* **89**, 250404 (2002).
- [56] S. D. Huber, E. Altman, H. P. Büchler, and G. Blatter, *Phys. Rev. B* **75**, 085106 (2007).
- [57] K. Nagao and I. Danshita, *Prog. Theor. Exp. Phys.* **2016**, 063101 (2016).
- [58] M. Schechter and T. Iadecola, *Phys. Rev. Lett.* **123**, 147201 (2019).
- [59] S. Chattopadhyay, H. Pichler, M. D. Lukin, and W. W. Ho, *Phys. Rev. B* **101**, 174308 (2020).
- [60] A. Kitazawa, K. Hijii, and K. Nomura, *J. Phys. A: Math. Gen.* **36**, L351 (2003).
- [61] P.-A. Lindgard and O. Danielsen, *J. Phys. C: Solid State Phys.*

- 7, 1523 (1974).
- [62] E. G. Batyev, Zh. Eksp. Teor. Fiz. **89**, 308 (1985).
- [63] G. Marmorini, D. Yamamoto, and I. Danshita, *Phys. Rev. B* **93**, 224402 (2016).
- [64] M. Vogl, P. Laurell, H. Zhang, S. Okamoto, and G. A. Fiete, *Phys. Rev. Res.* **2**, 043243 (2020).
- [65] J. König and A. Hucht, *SciPost Phys.* **10**, 7 (2021).
- [66] See the Supplemental Material.
- [67] A. R. Kolovsky and A. Buchleitner, *Europhy. Lett.* **68**, 632 (2004).
- [68] D. N. Page, *Phys. Rev. Lett.* **71**, 1291 (1993).
- [69] K. Tamura and H. Katsura, *Phys. Rev. B* **106**, 144306 (2022).
- [70] C. Cohen-Tannoudji, J. Dupont-Roc, and G. Grynberg, *Atom-Photon Interactions: Basic Processes and Applications* (Wiley-VCH, New York, 1998).
- [71] S. Bravyi, D. P. DiVincenzo, and D. Loss, *Ann. Phys. (NY)* **326**, 2793 (2011).
- [72] D. Petrosyan, B. Schmidt, J. R. Anglin, and M. Fleischhauer, *Phys. Rev. A* **76**, 033606 (2007).
- [73] A. Rosch, D. Rasch, B. Binz, and M. Vojta, *Phys. Rev. Lett.* **101**, 265301 (2008).
- [74] G. Carleo, F. Becca, M. Schiró, and M. Fabrizio, *Sci. Rep.* **2**, 243 (2012).
- [75] M. Kunimi and I. Danshita, *Phys. Rev. A* **104**, 043322 (2021).
- [76] A. J. Daley, J. M. Taylor, S. Diehl, M. Baranov, and P. Zoller, *Phys. Rev. Lett.* **102**, 040402 (2009).
- [77] M. J. Mark, E. Haller, K. Lauber, J. G. Danzl, A. Janisch, H. P. Büchler, A. J. Daley, and H.-C. Nägerl, *Phys. Rev. Lett.* **108**, 215302 (2012).
- [78] T. Kraemer, M. Mark, P. Waldburger, J. G. Danzl, C. Chin, B. Engeser, A. D. Lange, K. Pilch, A. Jaakkola, H.-C. Nägerl, and R. Grimm, *Nature* **440**, 315 (2006).
- [79] L. Tanzi, E. Lucioni, S. Chaudhuri, L. Gori, A. Kumar, C. D’Errico, M. Inguscio, and G. Modugno, *Phys. Rev. Lett.* **111**, 115301 (2013).
- [80] L. Tanzi, S. S. Abbate, F. Cataldini, L. Gori, E. Lucioni, M. Inguscio, G. Modugno, and C. D’Errico, *Sci. Rep.* **6**, 25965 (2016).
- [81] Y. Takasu, T. Yagami, H. Asaka, Y. Fukushima, K. Nagao, S. Goto, I. Danshita, and Y. Takahashi, *Sci. Adv.* **6**, eaba9255 (2020).
- [82] M. Cheneau, P. Barmettler, D. Poletti, M. Endres, P. Schauß, T. Fukuhara, C. Gross, I. Bloch, C. Kollath, and S. Kuhr, *Nature* **481**, 484 (2012).
- [83] R. Islam, R. Ma, P. M. Preiss, M. Eric Tai, A. Lukin, M. Rispoli, and M. Greiner, *Nature* **528**, 77 (2015).
- [84] A. M. Kaufman, M. E. Tai, A. Lukin, M. Rispoli, R. Schittko, P. M. Preiss, and M. Greiner, *Science* **353**, 794 (2016).
- [85] N. O’Dea, F. Burnell, A. Chandran, and V. Khemani, *Phys. Rev. Res.* **2**, 043305 (2020).
- [86] L.-H. Tang, N. O’Dea, and A. Chandran, *Phys. Rev. Res.* **4**, 043006 (2022).

Supplemental Material: Quantum many-body scars in the Bose-Hubbard model with a three-body constraint

Ryui Kaneko,^{1,2,3,*} Masaya Kunimi,^{4,†} and Ippei Danshita^{3,‡}

¹Waseda Research Institute for Science and Engineering, Waseda University, Shinjuku, Tokyo 169-8555, Japan

²Department of Engineering and Applied Sciences, Sophia University, Chiyoda, Tokyo 102-8554, Japan

³Department of Physics, Kindai University, Higashi-Osaka, Osaka 577-8502, Japan

⁴Department of Physics, Tokyo University of Science, Shinjuku, Tokyo 162-8601, Japan

(Dated: January 18, 2024)

CONTENTS

S-I. Scars in the constrained Bose-Hubbard model	1
A. Primitive proof that the quantum many-body scar states are the eigenstates of the constrained Bose-Hubbard model	1
B. Effects of boundary conditions and further-neighbor hoppings	2
C. Comment on the algebra of corresponding operators for the Bose-Hubbard model without any constraints	2
S-II. Correspondence between the spin and constrained Bose-Hubbard models	3
A. Generator of an SU(2) algebra for the $S = 1$ XY model	3
B. Mapping the interaction Hamiltonian	3
C. Zero-energy eigenstates of correlated hopping	4
D. Primitive proof that the quantum many-body scar states are the eigenstates of the correlated hopping terms	4
1. In the case of $\hat{H}_{\text{corr},1}$	4
2. In the case of $\hat{H}_{\text{corr},2}$	4
S-III. Analysis by the restricted spectrum generating algebra method	5
A. Restricted spectrum generating algebra of order one	6
B. Constrained Bose-Hubbard model with a conventional hopping term	6
C. With correlated hopping terms $\hat{H}_{\text{corr},1}$ and $\hat{H}_{\text{corr},2}$	6
D. Without the three-body constraint	7
S-IV. Numerical results	7
A. Nonintegrability of each model	7
B. Bipartite EE	9
C. Size dependence of the energy spectra	10
D. Effect of external potential	10
References	11

S-I. SCARS IN THE CONSTRAINED BOSE-HUBBARD MODEL

A. Primitive proof that the quantum many-body scar states are the eigenstates of the constrained Bose-Hubbard model

We will see that the following states

$$\hat{J}^+ = \sum_i \frac{(-1)^{r_i}}{\sqrt{2}} \hat{a}_i^2, \quad |S_n\rangle \propto (\hat{J}^+)^n |\Omega\rangle, \quad |\Omega\rangle = \bigotimes_i |2_i\rangle \quad (\text{S1})$$

correspond to the bosonic counterpart of athermal eigenstates found in the $S = 1$ XY model [S1].

To show that the state $|S_n\rangle$ is an eigenstate of the Hamiltonian

$$\hat{H} = \hat{H}_0 + \hat{H}_{\text{int}}, \quad (\text{S2})$$

$$\hat{H}_0 = -J \sum_i (\hat{a}_i^\dagger \hat{a}_{i+1} + \text{H.c.}), \quad \hat{H}_{\text{int}} = \frac{U}{2} \sum_i \hat{n}_i (\hat{n}_i - 1), \quad (\text{S3})$$

we work in the local basis characterized by the particle number, consisting of $|n_i\rangle = |0\rangle, |1\rangle, \text{ and } |2\rangle$. Then, it is easy to check $\hat{H}_{\text{int}}|S_n\rangle \propto |S_n\rangle$. Both repulsive ($U > 0$) and attractive ($U < 0$) interactions satisfy this relation. Hereafter, we will check that they are also eigenstates of \hat{H}_0 .

Let us first focus on the $n = 1$ case, where the state is

$$|S_1\rangle = \frac{1}{\sqrt{L}} (-|0222 \cdots 22\rangle + |2022 \cdots 22\rangle - |2202 \cdots 22\rangle + \cdots + (-1)^L |22 \cdots 20\rangle) \quad (\text{S4})$$

$$= \frac{1}{\sqrt{L}} \sum_i (-1)^{r_i} | \underbrace{22 \cdots 22}_{i-1} \underbrace{022 \cdots 22}_{L-i} \rangle. \quad (\text{S5})$$

For simplicity, we consider periodic boundary conditions. We will see later that same arguments hold for open boundary conditions. Since the maximum occupation number is $n_{\text{max}} = 2$, the noninteracting terms $(\hat{a}_{i-1}^\dagger \hat{a}_i + \hat{a}_i^\dagger \hat{a}_{i-1})$ and $(\hat{a}_i^\dagger \hat{a}_{i+1} + \hat{a}_{i+1}^\dagger \hat{a}_i)$ act on the state $|S_1\rangle$ in the following manner:

$$\begin{aligned} & (\hat{a}_{i-1}^\dagger \hat{a}_i + \hat{a}_i^\dagger \hat{a}_{i-1}) |S_1\rangle \\ &= (\hat{a}_{i-1}^\dagger \hat{a}_i + \hat{a}_i^\dagger \hat{a}_{i-1}) | \underbrace{22 \cdots 2}_{i-2} \underbrace{2022 \cdots 22}_{L-i-1} \rangle \\ &= \sqrt{2} | \underbrace{22 \cdots 2}_{i-2} \underbrace{1122 \cdots 22}_{L-i-1} \rangle \end{aligned} \quad (\text{S6})$$

* ryuikaneko@aoni.waseda.jp

† kunimi@rs.tus.ac.jp

‡ danshita@phys.kindai.ac.jp

and

$$\begin{aligned}
& (\hat{a}_i^\dagger \hat{a}_{i+1} + \hat{a}_{i+1}^\dagger \hat{a}_i) |S_1\rangle \\
&= (\hat{a}_i^\dagger \hat{a}_{i+1} + \hat{a}_{i+1}^\dagger \hat{a}_i) \underbrace{|22 \cdots 2}_{i-2} \underbrace{2022 \cdots 22}_{L-i-1}\rangle \\
&= \sqrt{2} \underbrace{|22 \cdots 2}_{i-2} \underbrace{2112 \cdots 22}_{L-i-1}\rangle. \tag{S7}
\end{aligned}$$

Here, any term represented as $|\underbrace{\cdots 2}_{i-1} \underbrace{\cdots}_{L-i}\rangle$ in $|S_1\rangle$ vanishes since $\hat{a}_i^\dagger |2_i\rangle = 0$. Then,

$$\begin{aligned}
\hat{H}_0 |S_1\rangle &\propto \frac{1}{\sqrt{L}} \sum_i (-1)^{r_i} \underbrace{|22 \cdots 2}_{i-2} \underbrace{1122 \cdots 22}_{L-i-1}\rangle \\
&\quad + \frac{1}{\sqrt{L}} \sum_i (-1)^{r_i} \underbrace{|22 \cdots 2}_{i-2} \underbrace{2112 \cdots 22}_{L-i-1}\rangle. \tag{S8}
\end{aligned}$$

By shifting $i \rightarrow i-1$ in the second term of the right-hand side, we have

$$\begin{aligned}
\hat{H}_0 |S_1\rangle &\propto \frac{1}{\sqrt{L}} \sum_i (-1)^{r_i} \underbrace{|22 \cdots 2}_{i-2} \underbrace{1122 \cdots 22}_{L-i-1}\rangle \\
&\quad + \frac{1}{\sqrt{L}} \sum_i (-1)^{r_{i-1}} \underbrace{|22 \cdots 2}_{i-3} \underbrace{2112 \cdots 22}_{L-i}\rangle \tag{S9} \\
&= \frac{1}{\sqrt{L}} \sum_i (-1)^{r_i} \underbrace{|22 \cdots 2}_{i-2} \underbrace{1122 \cdots 22}_{L-i-1}\rangle \\
&\quad - \frac{1}{\sqrt{L}} \sum_i (-1)^{r_i} \underbrace{|22 \cdots 2}_{i-2} \underbrace{1122 \cdots 22}_{L-i-1}\rangle = 0. \tag{S10}
\end{aligned}$$

Therefore, $|S_1\rangle$ is a zero-energy eigenstate of \hat{H}_0 .

For $n = 2$, the state is given as

$$\begin{aligned}
|S_2\rangle &= \frac{1}{\sqrt{L(L-1)/2}} (-|002222 \cdots 222\rangle \\
&\quad + |020222 \cdots 222\rangle - |022022 \cdots 222\rangle + \cdots \\
&\quad - |200222 \cdots 222\rangle + |202022 \cdots 222\rangle + \cdots \\
&\quad + (-1)^{2L-1} |22 \cdots 200\rangle) \tag{S11} \\
&= \frac{1}{\sqrt{L(L-1)/2}} \sum_i \left[-\underbrace{|22 \cdots 22}_{i-1} \underbrace{00}_{L-i-1} \underbrace{22 \cdots 22}_{L-i-1}\rangle \right. \\
&\quad \left. + \sum_{j \neq 1} (-1)^{r_j} \underbrace{|22 \cdots 22}_{i-1} \underbrace{0}_{j-1} \underbrace{22 \cdots 22}_{L-i-j} \underbrace{0}_{L-i-j} \underbrace{22 \cdots 22}_{L-i-j}\rangle \right]. \tag{S12}
\end{aligned}$$

Let us discuss how part of the noninteracting term acts on each term of $|S_2\rangle$. For example, since $\hat{a}|0\rangle = \hat{a}^\dagger|2\rangle = 0$, it is clear that

$$(\hat{a}_i^\dagger \hat{a}_{i+1} + \hat{a}_{i+1}^\dagger \hat{a}_i) \underbrace{|\cdots 00}_{i-1} \underbrace{\cdots}_{L-i-1}\rangle = 0, \tag{S13}$$

$$(\hat{a}_i^\dagger \hat{a}_{i+1} + \hat{a}_{i+1}^\dagger \hat{a}_i) \underbrace{|\cdots 22}_{i-1} \underbrace{\cdots}_{L-i-1}\rangle = 0. \tag{S14}$$

Because $|S_2\rangle$ is antisymmetrized, the sign of the state $|\underbrace{\cdots 02}_{i-1} \underbrace{\cdots}_{L-i-1}\rangle$ is opposite to that of the state

$|\underbrace{\cdots 20}_{i-1} \underbrace{\cdots}_{L-i-1}\rangle$. By acting the noninteracting term to the linear combination of these two states, we obtain

$$\begin{aligned}
& (\hat{a}_i^\dagger \hat{a}_{i+1} + \hat{a}_{i+1}^\dagger \hat{a}_i) (|\underbrace{\cdots 02}_{i-1} \underbrace{\cdots}_{L-i-1}\rangle - |\underbrace{\cdots 20}_{i-1} \underbrace{\cdots}_{L-i-1}\rangle) \\
&= \sqrt{2} (|\underbrace{\cdots 11}_{i-1} \underbrace{\cdots}_{L-i-1}\rangle - |\underbrace{\cdots 11}_{i-1} \underbrace{\cdots}_{L-i-1}\rangle) = 0. \tag{S15}
\end{aligned}$$

Therefore, $(\hat{a}_i^\dagger \hat{a}_{i+1} + \hat{a}_{i+1}^\dagger \hat{a}_i) |S_2\rangle = 0$ holds for any site i . Thus, the state $|S_2\rangle$ is the zero-energy eigenstate of \hat{H}_0 .

For general n , the state is given as

$$|S_n\rangle = \sum_{i_1 \neq \cdots \neq i_n} \frac{(-1)^{r_{i_1} + \cdots + r_{i_n}}}{\binom{L}{n}^{1/2}} \bigotimes_j |j\rangle, \quad \begin{cases} |0_j\rangle, & j \in \{i_1, \dots, i_n\}, \\ |2_j\rangle, & \text{otherwise.} \end{cases} \tag{S16}$$

Repeating the same procedure as in the case of $n = 2$, it is clear that the state $|S_n\rangle$ is the zero-energy eigenstate of \hat{H}_0 . Note that the mechanism of the quantum many-body scar (QMBS) states can also be understood by a restricted spectrum generating algebra (RSGA) [S2] (see Sec. S-III for more details).

The athermal behavior of the eigenstate $|S_{n=L/2}\rangle$ is closely related to the nonergodic dynamics after a quantum quench starting from the charge-density-wave (CDW) initial state $|\cdots 2020 \cdots\rangle$ to a strongly interacting regime in the 1D Bose-Hubbard model at unit filling [S3]. The state $|S_{L/2}\rangle$ is a linear combination of CDW states, consisting of $L/2$ $|0\rangle$'s and $L/2$ $|2\rangle$'s. The maximum particle number per site effectively becomes $n_{\max} = 2$ in the strong-coupling limit, and this CDW initial state has a small but nonzero overlap $\binom{L}{L/2}^{-1/2} \approx \sqrt{\pi L/2} \times 2^{-L}$ with the athermal state $|S_{n=L/2}\rangle$.

B. Effects of boundary conditions and further-neighbor hoppings

As was discussed in the previous studies [S1, S4], because the same arguments hold without the $(\hat{a}_L^\dagger \hat{a}_1 + \hat{a}_1^\dagger \hat{a}_L)$ term, what we have shown here is valid for open boundary conditions as well. Adding further-neighbor hoppings at odd distances apart J_3, J_5, J_7, \dots and adding a chemical potential term do not change the arguments either. These states can be athermal eigenstates even when the hopping has randomness.

C. Comment on the algebra of corresponding operators for the Bose-Hubbard model without any constraints

When the local Hilbert space is not truncated ($n_{\max} \rightarrow \infty$), relevant operators fulfill an $SU(1, 1)$ algebra [S5, S6] for which

the corresponding operators satisfy $[\hat{L}^+, \hat{L}^-] = -2\hat{L}^z$ [the sign on the right-hand side is negative in contrast to the SU(2) algebra] and $[\hat{L}^z, \hat{L}^\pm] = \pm\hat{L}^\pm$. In this case, we define the ladder operators

$$\hat{L}^+ = \frac{1}{2} \sum_i (-1)^{r_i} (\hat{b}_i^\dagger)^2, \quad \hat{L}^- = \frac{1}{2} \sum_i (-1)^{r_i} \hat{b}_i^2, \quad (\text{S17})$$

where the role of creation and annihilation operators is reversed and the prefactor changes from $1/\sqrt{2}$ to $1/2$ compared to the SU(2) case. Using the commutation relation $[\hat{b}_i^\dagger, (\hat{b}_j^\dagger)^2] = (4\hat{b}_i^\dagger \hat{b}_i + 2)\delta_{ij}$, we obtain

$$\hat{L}^z = -\frac{1}{2} [\hat{L}^+, \hat{L}^-] = \frac{1}{2} \sum_i \left(\hat{b}_i^\dagger \hat{b}_i + \frac{1}{2} \right). \quad (\text{S18})$$

It is easy to show the commutation relation $[\hat{L}^z, \hat{L}^\pm] = \pm\hat{L}^\pm$ using the relations $[\hat{b}_i^\dagger \hat{b}_i, \hat{b}_j^2] = -2\hat{b}_i^2 \delta_{ij}$ and $[\hat{b}_i^\dagger \hat{b}_i, (\hat{b}_j^\dagger)^2] = 2(\hat{b}_i^\dagger)^2 \delta_{ij}$.

S-II. CORRESPONDENCE BETWEEN THE SPIN AND CONSTRAINED BOSE-HUBBARD MODELS

We have constructed the exact QMBS states in the Bose-Hubbard model with a three-body constraint in the previous section. To clarify the correspondence between the QMBS states in the Bose-Hubbard and $S = 1$ spin models, we transform the spin model into the Bose-Hubbard-like model exactly. According to the improved Holstein-Primakoff expansion [S7–S11], the matrix representation of the $S = 1$ spin operator $\hat{S}^+ = \hat{S}^x + i\hat{S}^y$ is obtained in the local Hilbert space spanned by the unconstrained boson basis $\{|0\rangle, |1\rangle, |2\rangle, |3\rangle, |4\rangle, |5\rangle, \dots\}$ as

$$\hat{S}^+ = \sqrt{2}\hat{b} + (1 - \sqrt{2})\hat{b}^\dagger \hat{b}^2 + \left(\frac{1}{\sqrt{2}} - 1 \right) (\hat{b}^\dagger)^2 \hat{b}^3 \quad (\text{S19})$$

$$\rightarrow \begin{pmatrix} 0 & \sqrt{2} & 0 & 0 & 0 & 0 & \dots \\ 0 & 0 & \sqrt{2} & 0 & 0 & 0 & \dots \\ 0 & 0 & 0 & 0 & 0 & 0 & \dots \\ 0 & 0 & 0 & 0 & -6 + 2\sqrt{2} & 0 & \dots \\ 0 & 0 & 0 & 0 & 0 & -8\sqrt{5} + 3\sqrt{10} & \dots \\ 0 & 0 & 0 & 0 & 0 & 0 & \dots \\ \vdots & \vdots & \vdots & \vdots & \vdots & \vdots & \ddots \end{pmatrix}. \quad (\text{S20})$$

Note that the matrix elements that are colored gray, connecting the physical and unphysical subspaces, are all zero. In the main text, we find that the transformed Bose-Hubbard-like model contains additional terms, which share the same QMBS states defined in Eq. (S1).

A. Generator of an SU(2) algebra for the $S = 1$ XY model

Let us first briefly review the QMBS states in the $S = 1$ XY model on a chain [S1, S4]. They exist in the model given as

$$\hat{H}^{XY} = \hat{H}_0^{XY} + \hat{H}_{\text{int}}^{XY}, \quad (\text{S21})$$

$$\hat{H}_0^{XY} = J_{xy} \sum_i (\hat{S}_i^x \hat{S}_{i+1}^x + \hat{S}_i^y \hat{S}_{i+1}^y), \quad (\text{S22})$$

$$\hat{H}_{\text{int}}^{XY} = H_z \sum_i \hat{S}_i^z + D_z \sum_i (\hat{S}_i^z)^2, \quad (\text{S23})$$

where \hat{S}^α ($\alpha = x, y, z$) denotes the $S = 1$ spin operator, J_{xy} is the strength of the transverse spin exchange interaction, H_z is the strength of the magnetic field, and D_z is the strength of the single-ion anisotropy. We choose open or periodic boundary conditions in Eqs. (S22) and (S23). The ladder operators

$$\hat{K}^\pm = \frac{1}{2} \sum_i (-1)^{r_i} (\hat{S}_i^\pm)^2, \quad (\text{S24})$$

$$\hat{K}^z = \frac{1}{2} \sum_i \hat{S}_i^z \quad (\text{S25})$$

with $\hat{S}_i^\pm = \hat{S}_i^x \pm i\hat{S}_i^y$ were introduced [S1, S4, S12] to study the SU(2) symmetry characterized by

$$[\hat{K}^+, \hat{K}^-] = 2\hat{K}^z, \quad [\hat{K}^z, \hat{K}^\pm] = \pm\hat{K}^\pm. \quad (\text{S26})$$

The related QMBS states are generated as

$$|\tilde{S}_n\rangle \propto (\hat{K}^+)^n |\tilde{\Omega}\rangle, \quad |\tilde{\Omega}\rangle = \bigotimes_i |m_i = -1\rangle, \quad (\text{S27})$$

which satisfy $\hat{H}_0^{XY} |\tilde{S}_n\rangle = 0$ and $\hat{H}_{\text{int}}^{XY} |\tilde{S}_n\rangle \propto |\tilde{S}_n\rangle$. They exhibit a subextensive entanglement entropy (EE) growth at most logarithmically with system size.

B. Mapping the interaction Hamiltonian

Hereafter, we focus on the truncated Hilbert space $n_{\text{max}} = 2$ and replace all the bosonic operators \hat{b}_i with \hat{a}_i for simplicity. The remaining terms in Eq. (S23) can be obtained using the relation

$$\hat{S}_i^z = S - \hat{a}_i^\dagger \hat{a}_i = \frac{n_{\text{max}}}{2} - \hat{a}_i^\dagger \hat{a}_i. \quad (\text{S28})$$

For the periodic boundary condition, they become

$$\begin{aligned} \hat{H}_{\text{int}}^{XY} &= D_z \sum_i \hat{n}_i^2 - (D_z n_{\text{max}} + H_z) \sum_i \hat{n}_i \\ &+ \left(D_z \frac{n_{\text{max}}^2}{4} + H_z \frac{n_{\text{max}}}{2} \right) \sum_i 1. \end{aligned} \quad (\text{S29})$$

Comparing it with the Bose-Hubbard model up to a constant, we have

$$\hat{H}'_{\text{int}} = \frac{U}{2} \sum_i \hat{n}_i (\hat{n}_i - 1) - \mu \sum_i \hat{n}_i \quad (\text{S30})$$

$$= \frac{U}{2} \sum_i \hat{n}_i^2 - \left(\frac{U}{2} + \mu \right) \sum_i \hat{n}_i \quad (\text{S31})$$

with

$$U = 2D_z, \quad (\text{S32})$$

$$\mu = D_z (n_{\text{max}} - 1) + H_z. \quad (\text{S33})$$

C. Zero-energy eigenstates of correlated hopping

Here, we will demonstrate that each correlated hopping term

$$\begin{aligned} \hat{H}_0^{XY} &= J_{xy} \sum_i (\hat{a}_i \hat{a}_{i+1}^\dagger + \text{H.c.}) \\ &+ \left(\frac{1}{\sqrt{2}} - 1 \right) J_{xy} \sum_i (\hat{a}_i \hat{a}_{i+1}^\dagger \hat{n}_{i+1} + \hat{a}_{i+1} \hat{a}_i^\dagger \hat{n}_i + \text{H.c.}) \\ &+ \left(\frac{3}{2} - \sqrt{2} \right) J_{xy} \sum_i (\hat{n}_i \hat{a}_i \hat{a}_{i+1}^\dagger \hat{n}_{i+1} + \text{H.c.}), \end{aligned} \quad (\text{S34})$$

obtained in the main text, possesses the QMBS states defined in Eq. (S1).

We focus on the generalized Bose-Hubbard Hamiltonian

$$\hat{H}^{\text{Hub}} = \hat{H}_0 + \hat{H}_{\text{corr},1} + \hat{H}_{\text{corr},2} + \hat{H}'_{\text{int}}, \quad (\text{S35})$$

where the middle two terms on the right-hand side are defined as

$$\hat{H}_{\text{corr},1} = -J_{\text{corr},1} \sum_i \left(\hat{a}_i \hat{a}_{i+1}^\dagger \hat{n}_{i+1} + \hat{a}_{i+1} \hat{a}_i^\dagger \hat{n}_i + \text{H.c.} \right), \quad (\text{S36})$$

$$\hat{H}_{\text{corr},2} = -J_{\text{corr},2} \sum_i (\hat{n}_i \hat{a}_i \hat{a}_{i+1}^\dagger \hat{n}_{i+1} + \text{H.c.}) \quad (\text{S37})$$

while \hat{H}_0 and \hat{H}'_{int} are defined in Eq. (S3) and Eq. (S30), respectively. The original $S = 1$ XY model [see Eqs. (S21)–(S23)] is reproduced when we choose

$$J = -J_{xy}, \quad (\text{S38})$$

$$J_{\text{corr},1} = -\left(\frac{1}{\sqrt{2}} - 1 \right) J_{xy}, \quad (\text{S39})$$

$$J_{\text{corr},2} = -\left(\frac{3}{2} - \sqrt{2} \right) J_{xy}. \quad (\text{S40})$$

On the other hand, when the strengths of the correlated hoppings $J_{\text{corr},1}$ and $J_{\text{corr},2}$ are chosen independently, there will be no direct correspondence between the $S = 1$ XY model and the Bose-Hubbard model.

As we have shown in Sec. S-II B, with a three-body constraint satisfying $n_{\text{max}} = 2$, both the Bose-Hubbard model and the $S = 1$ XY model share the equivalent athermal state $|S_n\rangle$, i.e.,

$$\hat{H}_0 |S_n\rangle = 0, \quad (\text{S41})$$

$$(\hat{H}_0 + \hat{H}_{\text{corr},1} + \hat{H}_{\text{corr},2}) |S_n\rangle = 0, \quad (\text{S42})$$

$$\hat{H}'_{\text{int}} |S_n\rangle \propto |S_n\rangle \quad (\text{S43})$$

when Eqs. (S38)–(S40) hold. From this, the relation

$$(\hat{H}_{\text{corr},1} + \hat{H}_{\text{corr},2}) |S_n\rangle = 0 \quad (\text{S44})$$

clearly holds. We may further expect that the state $|S_n\rangle$ is also the zero-energy eigenstate of each of the correlated hopping terms $\hat{H}_{\text{corr},1}$ and $\hat{H}_{\text{corr},2}$, i.e.,

$$\hat{H}_{\text{corr},1} |S_n\rangle = \hat{H}_{\text{corr},2} |S_n\rangle = 0, \quad (\text{S45})$$

irrespective of the strength of the correlated hopping $J_{\text{corr},1}$ or $J_{\text{corr},2}$. This expectation is indeed true as we will prove in Sec. S-II D. This result suggests that the QMBS states exist in a wide range of parameter regions for the Bose-Hubbard-like model, as well as in the constrained Bose-Hubbard model with a conventional hopping term and in that with the correlated hopping terms corresponding to the $S = 1$ XY model. Note that other types of QMBS states in the presence of these correlated hoppings were also studied recently [S13, S14], separately from the interest in the $S = 1$ XY model.

D. Primitive proof that the quantum many-body scar states are the eigenstates of the correlated hopping terms

We show that the QMBS states of the constrained Bose-Hubbard model with the conventional hopping term are the eigenstates of the correlated hopping terms. (As for the relation to the RSGA, see also Sec. S-III.)

1. In the case of $\hat{H}_{\text{corr},1}$

Here, we will show that $|S_n\rangle$ is a zero-energy eigenstate of $\hat{H}_{\text{corr},1}$.

For $n = 1$, each term in $\hat{H}_{\text{corr},1}$ acts on the state $|S_1\rangle = \frac{1}{\sqrt{L}} \sum_i (-1)^{r_i} | \underbrace{22 \cdots 22}_i \underbrace{22 \cdots 22}_{L-i} \rangle$ in the following manner:

$$\begin{aligned} &(\hat{a}_{i-1} \hat{a}_i^\dagger \hat{n}_i + \hat{n}_i \hat{a}_i \hat{a}_{i-1}^\dagger) |S_1\rangle \\ &= (\hat{a}_{i-1} \hat{a}_i^\dagger \hat{n}_i + \hat{n}_i \hat{a}_i \hat{a}_{i-1}^\dagger) | \underbrace{22 \cdots 2}_{i-2} \underbrace{2022 \cdots 22}_{L-i-1} \rangle = 0, \end{aligned} \quad (\text{S46})$$

$$\begin{aligned} &(\hat{a}_i \hat{a}_{i+1}^\dagger \hat{n}_{i+1} + \hat{n}_{i+1} \hat{a}_{i+1} \hat{a}_i^\dagger) |S_1\rangle \\ &= (\hat{a}_i \hat{a}_{i+1}^\dagger \hat{n}_{i+1} + \hat{n}_{i+1} \hat{a}_{i+1} \hat{a}_i^\dagger) | \underbrace{22 \cdots 2}_{i-2} \underbrace{2022 \cdots 22}_{L-i-1} \rangle \\ &= \sqrt{2} | \underbrace{22 \cdots 2}_{i-2} \underbrace{2112 \cdots 22}_{L-i-1} \rangle, \end{aligned} \quad (\text{S47})$$

$$\begin{aligned} &(\hat{a}_i \hat{a}_{i-1}^\dagger \hat{n}_{i-1} + \hat{n}_{i-1} \hat{a}_{i-1} \hat{a}_i^\dagger) |S_1\rangle \\ &= (\hat{a}_i \hat{a}_{i-1}^\dagger \hat{n}_{i-1} + \hat{n}_{i-1} \hat{a}_{i-1} \hat{a}_i^\dagger) | \underbrace{22 \cdots 2}_{i-2} \underbrace{2022 \cdots 22}_{L-i-1} \rangle \\ &= \sqrt{2} | \underbrace{22 \cdots 2}_{i-2} \underbrace{1122 \cdots 22}_{L-i-1} \rangle, \end{aligned} \quad (\text{S48})$$

$$\begin{aligned} &(\hat{a}_{i+1} \hat{a}_i^\dagger \hat{n}_i + \hat{n}_i \hat{a}_i \hat{a}_{i+1}^\dagger) |S_1\rangle \\ &= (\hat{a}_{i+1} \hat{a}_i^\dagger \hat{n}_i + \hat{n}_i \hat{a}_i \hat{a}_{i+1}^\dagger) | \underbrace{22 \cdots 2}_{i-2} \underbrace{2022 \cdots 22}_{L-i-1} \rangle = 0. \end{aligned} \quad (\text{S49})$$

Here, any term represented as $| \cdots \underbrace{2}_{i-1} \cdots \underbrace{}_{L-i} \rangle$ in $|S_1\rangle$ vanishes

since $\hat{a}_i^\dagger |2_i\rangle = 0$. Then,

$$\hat{H}_{\text{corr},1} |S_1\rangle \propto \frac{1}{\sqrt{L}} \sum_i (-1)^{r_i} | \underbrace{22 \cdots 2}_{i-2} \underbrace{1122 \cdots 22}_{L-i-1} \rangle$$

$$+ \frac{1}{\sqrt{L}} \sum_i (-1)^{r_i} \underbrace{|22 \cdots 2}_{i-2} \underbrace{2111}_{L-i-1} |2 \cdots 22\rangle. \quad (\text{S50})$$

As in the case of \hat{H}_0 , by shifting $i \rightarrow i-1$ in the second term of the right-hand side, the first and second terms cancel each other out. Thus, $|S_1\rangle$ is a zero-energy eigenstate of $\hat{H}_{\text{corr},1}$.

For $n=2$, as in the case of \hat{H}_0 , we consider how part of the noninteracting term acts on each term of $|S_2\rangle$. First, it is clear that

$$(\hat{a}_i \hat{a}_{i+1}^\dagger \hat{n}_{i+1} + \hat{n}_{i+1} \hat{a}_{i+1} \hat{a}_i^\dagger) | \underbrace{\cdots 00}_{i-1} \underbrace{\cdots}_{L-i-1} \rangle = 0, \quad (\text{S51})$$

$$(\hat{a}_i \hat{a}_{i+1}^\dagger \hat{n}_{i+1} + \hat{n}_{i+1} \hat{a}_{i+1} \hat{a}_i^\dagger) | \underbrace{\cdots 22}_{i-1} \underbrace{\cdots}_{L-i-1} \rangle = 0, \quad (\text{S52})$$

$$(\hat{a}_{i+1} \hat{a}_i^\dagger \hat{n}_i + \hat{n}_i \hat{a}_i \hat{a}_{i+1}^\dagger) | \underbrace{\cdots 00}_{i-1} \underbrace{\cdots}_{L-i-1} \rangle = 0, \quad (\text{S53})$$

$$(\hat{a}_{i+1} \hat{a}_i^\dagger \hat{n}_i + \hat{n}_i \hat{a}_i \hat{a}_{i+1}^\dagger) | \underbrace{\cdots 22}_{i-1} \underbrace{\cdots}_{L-i-1} \rangle = 0. \quad (\text{S54})$$

Then, we focus on terms $| \underbrace{\cdots 02}_{i-1} \underbrace{\cdots}_{L-i-1} \rangle$ and $| \underbrace{\cdots 20}_{i-1} \underbrace{\cdots}_{L-i-1} \rangle$, whose coefficients have the opposite sign due to the antisymmetrization of $|S_2\rangle$. A straightforward calculation yields

$$\begin{aligned} & (\hat{a}_i \hat{a}_{i+1}^\dagger \hat{n}_{i+1} + \hat{n}_{i+1} \hat{a}_{i+1} \hat{a}_i^\dagger) \\ & \cdot (| \underbrace{\cdots 02}_{i-1} \underbrace{\cdots}_{L-i-1} \rangle - | \underbrace{\cdots 20}_{i-1} \underbrace{\cdots}_{L-i-1} \rangle) \\ & = \sqrt{2} | \underbrace{\cdots 11}_{i-1} \underbrace{\cdots}_{L-i-1} \rangle, \end{aligned} \quad (\text{S55})$$

$$\begin{aligned} & (\hat{a}_{i+1} \hat{a}_i^\dagger \hat{n}_i + \hat{n}_i \hat{a}_i \hat{a}_{i+1}^\dagger) \\ & \cdot (| \underbrace{\cdots 02}_{i-1} \underbrace{\cdots}_{L-i-1} \rangle - | \underbrace{\cdots 20}_{i-1} \underbrace{\cdots}_{L-i-1} \rangle) \\ & = -\sqrt{2} | \underbrace{\cdots 11}_{i-1} \underbrace{\cdots}_{L-i-1} \rangle, \end{aligned} \quad (\text{S56})$$

$$\begin{aligned} \therefore & (\hat{a}_i \hat{a}_{i+1}^\dagger \hat{n}_{i+1} + \hat{n}_{i+1} \hat{a}_{i+1} \hat{a}_i^\dagger + \hat{a}_{i+1} \hat{a}_i^\dagger \hat{n}_i + \hat{n}_i \hat{a}_i \hat{a}_{i+1}^\dagger) \\ & \cdot (| \underbrace{\cdots 02}_{i-1} \underbrace{\cdots}_{L-i-1} \rangle - | \underbrace{\cdots 20}_{i-1} \underbrace{\cdots}_{L-i-1} \rangle) = 0. \end{aligned} \quad (\text{S57})$$

Therefore, $(\hat{a}_i \hat{a}_{i+1}^\dagger \hat{n}_{i+1} + \hat{n}_{i+1} \hat{a}_{i+1} \hat{a}_i^\dagger + \hat{a}_{i+1} \hat{a}_i^\dagger \hat{n}_i + \hat{n}_i \hat{a}_i \hat{a}_{i+1}^\dagger) |S_2\rangle = 0$ for any site i . Thus, the state $|S_2\rangle$ is the zero-energy eigenstate of $\hat{H}_{\text{corr},1}$.

Repeating the same procedure as in the case of $n=2$, we can show that the state $|S_n\rangle$ is the zero-energy eigenstate of $\hat{H}_{\text{corr},1}$ for $n > 2$.

2. In the case of $\hat{H}_{\text{corr},1}$

Likewise, we can show that $|S_n\rangle$ is a zero-energy eigenstate of $\hat{H}_{\text{corr},2}$.

For $n=1$, each term in $\hat{H}_{\text{corr},2}$ acts on the state $|S_1\rangle = \frac{1}{\sqrt{L}} \sum_i (-1)^{r_i} | \underbrace{22 \cdots 22}_{i-1} \underbrace{022 \cdots 22}_{L-i} \rangle$ in the following manner:

$$\begin{aligned} & (\hat{n}_{i-1} \hat{a}_{i-1} \hat{a}_i^\dagger \hat{n}_i + \hat{n}_i \hat{a}_i \hat{a}_{i-1}^\dagger \hat{n}_{i-1}) |S_1\rangle \\ & = (\hat{n}_{i-1} \hat{a}_{i-1} \hat{a}_i^\dagger \hat{n}_i + \hat{n}_i \hat{a}_i \hat{a}_{i-1}^\dagger \hat{n}_{i-1}) \\ & \quad \cdot | \underbrace{22 \cdots 2}_{i-2} \underbrace{2022}_{L-i-1} \cdots 22 \rangle \\ & = 0, \end{aligned} \quad (\text{S58})$$

and

$$\begin{aligned} & (\hat{n}_i \hat{a}_i \hat{a}_{i+1}^\dagger \hat{n}_{i+1} + \hat{n}_{i+1} \hat{a}_{i+1} \hat{a}_i^\dagger \hat{n}_i) |S_1\rangle \\ & = (\hat{n}_i \hat{a}_i \hat{a}_{i+1}^\dagger \hat{n}_{i+1} + \hat{n}_{i+1} \hat{a}_{i+1} \hat{a}_i^\dagger \hat{n}_i) \\ & \quad \cdot | \underbrace{22 \cdots 2}_{i-2} \underbrace{2022}_{L-i-1} \cdots 22 \rangle \\ & = 0. \end{aligned} \quad (\text{S59})$$

Here, any term represented as $| \underbrace{\cdots 2}_{i-1} \underbrace{\cdots}_{L-i} \rangle$ in $|S_1\rangle$ vanishes since $\hat{a}_i^\dagger |2_i\rangle = 0$. Therefore, acting any Hermitian term in $\hat{H}_{\text{corr},2}$ to $|S_1\rangle$ gives 0, and hence, $|S_1\rangle$ is a zero-energy eigenstate of $\hat{H}_{\text{corr},2}$.

For $n=2$, as in the cases of \hat{H}_0 and $\hat{H}_{\text{corr},1}$, we consider how part of the noninteracting term acts on each term of $|S_2\rangle$. First, it is clear that

$$(\hat{n}_i \hat{a}_i \hat{a}_{i+1}^\dagger \hat{n}_{i+1} + \hat{n}_{i+1} \hat{a}_{i+1} \hat{a}_i^\dagger \hat{n}_i) | \underbrace{\cdots 00}_{i-1} \underbrace{\cdots}_{L-i-1} \rangle = 0, \quad (\text{S60})$$

$$(\hat{n}_i \hat{a}_i \hat{a}_{i+1}^\dagger \hat{n}_{i+1} + \hat{n}_{i+1} \hat{a}_{i+1} \hat{a}_i^\dagger \hat{n}_i) | \underbrace{\cdots 22}_{i-1} \underbrace{\cdots}_{L-i-1} \rangle = 0. \quad (\text{S61})$$

Then, we focus on terms $| \underbrace{\cdots 02}_{i-1} \underbrace{\cdots}_{L-i-1} \rangle$ and $| \underbrace{\cdots 20}_{i-1} \underbrace{\cdots}_{L-i-1} \rangle$, whose coefficients have the opposite sign. Again, a straightforward calculation yields

$$\begin{aligned} & (\hat{n}_i \hat{a}_i \hat{a}_{i+1}^\dagger \hat{n}_{i+1} + \hat{n}_{i+1} \hat{a}_{i+1} \hat{a}_i^\dagger \hat{n}_i) \\ & \cdot (| \underbrace{\cdots 02}_{i-1} \underbrace{\cdots}_{L-i-1} \rangle - | \underbrace{\cdots 20}_{i-1} \underbrace{\cdots}_{L-i-1} \rangle) = 0. \end{aligned} \quad (\text{S62})$$

Therefore, $(\hat{n}_i \hat{a}_i \hat{a}_{i+1}^\dagger \hat{n}_{i+1} + \hat{n}_{i+1} \hat{a}_{i+1} \hat{a}_i^\dagger \hat{n}_i) |S_2\rangle = 0$ for any site i . Thus, the state $|S_2\rangle$ is the zero-energy eigenstate of $\hat{H}_{\text{corr},2}$.

Repeating the same procedure as in the case of $n=2$, $\hat{H}_{\text{corr},2} |S_n\rangle = 0$ holds for $n > 2$.

S-III. ANALYSIS BY THE RESTRICTED SPECTRUM GENERATING ALGEBRA METHOD

The mechanism of the QMBS states is well understood by an RSGA [S2]. In this section, we briefly review the concept of RSGA and how it is satisfied in the case of our models.

A. Restricted spectrum generating algebra of order one

Let us consider the Hamiltonian \hat{H}_0 , its eigenstate $|\psi_0\rangle$, and the operator \hat{Q}^\dagger satisfying $\hat{Q}^\dagger|\psi_0\rangle \neq 0$. If the conditions

$$\hat{H}_0|\psi_0\rangle = E_0|\psi_0\rangle, \quad (\text{S63})$$

$$[\hat{H}_0, \hat{Q}^\dagger]|\psi_0\rangle = \mathcal{E}\hat{Q}^\dagger|\psi_0\rangle, \quad (\text{S64})$$

$$[[\hat{H}_0, \hat{Q}^\dagger], \hat{Q}^\dagger] = 0 \quad (\text{S65})$$

hold, the Hamiltonian \hat{H}_0 is said to exhibit the restricted spectrum generating algebra of order one (RSGA-1) [S2].

It is known that the eigenstates generated by the RSGA are the QMBS states [S2]. In particular, for any state

$$|\psi_n\rangle := (\hat{Q}^\dagger)^n|\psi_0\rangle (\neq 0), \quad (\text{S66})$$

the relation

$$\hat{H}_0|\psi_n\rangle = (E_0 + n\mathcal{E})|\psi_n\rangle \quad (\text{S67})$$

holds. In general, to confirm the presence of the QMBS states, we have only to examine whether the Hamiltonian satisfies the conditions in Eqs. (S63)–(S65).

Hereafter, we will check how our models satisfy the RSGA-1.

B. Constrained Bose-Hubbard model with a conventional hopping term

We first consider the Hamiltonian $\hat{H} = \hat{H}_0 + \hat{H}_{\text{int}}$ given in Eq. (S2) under open or periodic boundary conditions. When we choose

$$|\psi_0\rangle = |22 \cdots 22\rangle, \quad (\text{S68})$$

it satisfies

$$\hat{H}|\psi_0\rangle = LU|\psi_0\rangle. \quad (\text{S69})$$

We then calculate the commutators $[\hat{H}_0, \hat{J}^+]$ and $[\hat{H}_{\text{int}}, \hat{J}^+]$. For this purpose, we write each operator as

$$\hat{a}_j = |0_j\rangle\langle 1_j| + \sqrt{2}|1_j\rangle\langle 2_j|, \quad (\text{S70})$$

$$\hat{a}_j^\dagger = |1_j\rangle\langle 0_j| + \sqrt{2}|2_j\rangle\langle 1_j|, \quad (\text{S71})$$

$$\hat{a}_j^2 = \sqrt{2}|0_j\rangle\langle 2_j|, \quad (\text{S72})$$

$$\hat{n}_j = |1_j\rangle\langle 1_j| + 2|2_j\rangle\langle 2_j| \quad (\text{S73})$$

and derive the commutation relations

$$[\hat{a}_{j+1}^\dagger \hat{a}_j, \hat{a}_k^2] = (-2|0_{j+1}\rangle\langle 1_{j+1}| + \sqrt{2}|1_{j+1}\rangle\langle 2_{j+1}|)\hat{a}_j \delta_{j+1,k}, \quad (\text{S74})$$

$$[\hat{a}_j^\dagger \hat{a}_{j+1}, \hat{a}_k^2] = (-2|0_j\rangle\langle 1_j| + \sqrt{2}|1_j\rangle\langle 2_j|)\hat{a}_{j+1} \delta_{jk}, \quad (\text{S75})$$

$$[\hat{n}_j, \hat{a}_k^2] = -2\hat{a}_j^2 \delta_{jk}, \quad (\text{S76})$$

$$[\hat{n}_j^2, \hat{a}_k^2] = -4\hat{a}_j^2 \delta_{jk}. \quad (\text{S77})$$

By defining the two-site operator

$$\hat{h}_{ij} = |1_i 0_j\rangle\langle 2_i 1_j| - |0_i 1_j\rangle\langle 1_i 2_j| \quad (\text{S78})$$

and using the aforementioned relations, we can simplify the commutator as

$$[\hat{H}_0, \hat{J}^+] = -3J \sum_j (-1)^j \hat{h}_{j,j+1}, \quad (\text{S79})$$

$$[\hat{H}_{\text{int}}, \hat{J}^+] = -U\hat{J}^+. \quad (\text{S80})$$

Since $\hat{h}_{j,j+1}|\psi_0\rangle = 0$, we obtain

$$[\hat{H}_0, \hat{J}^+]|\psi_0\rangle = 0, \quad (\text{S81})$$

and consequently,

$$[\hat{H}, \hat{J}^+]|\psi_0\rangle = -U\hat{J}^+|\psi_0\rangle. \quad (\text{S82})$$

Finally, because the commutation relations

$$[\hat{h}_{j,j+1}, \hat{a}_k^2 \hat{1}_{k+1}] = 0, \quad (\text{S83})$$

$$[\hat{h}_{j,j+1}, \hat{1}_k \hat{a}_{k+1}^2] = 0 \quad (\text{S84})$$

hold for any j and k , we get

$$[[\hat{H}, \hat{J}^+], \hat{J}^+] = 0. \quad (\text{S85})$$

Thus, the Hamiltonian \hat{H} satisfies the RSGA-1. The resulting QMBS states are represented as

$$|\psi_n\rangle \propto (\hat{J}^+)^n |22 \cdots 22\rangle, \quad (\text{S86})$$

$$\hat{H}|\psi_n\rangle = U(L-n)|\psi_n\rangle, \quad (\text{S87})$$

which are consistent with those obtained in the main text.

C. With correlated hopping terms $\hat{H}_{\text{corr},1}$ and $\hat{H}_{\text{corr},2}$

Next, we consider the Hamiltonian with the correlated hopping terms $\hat{H}_{\text{corr},1}$ and $\hat{H}_{\text{corr},2}$, which are given in Eq. (S36) and in Eq. (S37), respectively.

We can rewrite the Hamiltonians as

$$\hat{H}_{\text{corr},1} = -J_{\text{corr},1} \sum_j \hat{h}_{j,j+1}^{\text{corr},1}, \quad (\text{S88})$$

$$\begin{aligned} \hat{h}_{ij}^{\text{corr},1} := & 4|1_i 2_j\rangle\langle 2_i 1_j| + 4|2_i 1_j\rangle\langle 1_i 2_j| \\ & + \sqrt{2}(|0_i 2_j\rangle + |2_i 0_j\rangle)\langle 1_i 1_j| \\ & + \sqrt{2}|1_i 1_j\rangle(\langle 0_i 2_j| + \langle 2_i 0_j|) \end{aligned} \quad (\text{S89})$$

and

$$\hat{H}_{\text{corr},2} = -J_{\text{corr},2} \sum_j \hat{h}_{j,j+1}^{\text{corr},2}, \quad (\text{S90})$$

$$\hat{h}_{ij}^{\text{corr},2} := 2|1_i 2_j\rangle\langle 2_i 1_j| + 2|2_i 1_j\rangle\langle 1_i 2_j|. \quad (\text{S91})$$

Using these representations, we can show the relations

$$[\hat{h}_{j,j+1}^{\text{corr},1}, \hat{a}_j^2 \hat{1}_{j+1}] = 2|1_j 1_{j+1}\rangle\langle 2_j 2_{j+1}|$$

$$\begin{aligned}
& -2|0_j 0_{j+1}\rangle\langle 1_j 1_{j+1}| \\
& -4\sqrt{2}|0_j 1_{j+1}\rangle\langle 1_j 2_{j+1}|, \quad (\text{S92})
\end{aligned}$$

$$\begin{aligned}
[\hat{h}_{j,j+1}^{\text{corr},1}, \hat{1}_j \hat{a}_{j+1}^2] &= 2|1_j 1_{j+1}\rangle\langle 2_j 2_{j+1}| \\
& -2|0_j 0_{j+1}\rangle\langle 1_j 1_{j+1}| \\
& -4\sqrt{2}|1_j 0_{j+1}\rangle\langle 2_j 1_{j+1}| \quad (\text{S93})
\end{aligned}$$

and

$$[\hat{h}_{j,j+1}^{\text{corr},2}, \hat{a}_j^2 \hat{1}_{j+1}] = -2\sqrt{2}|0_j 1_{j+1}\rangle\langle 1_j 2_{j+1}|, \quad (\text{S94})$$

$$[\hat{h}_{j,j+1}^{\text{corr},2}, \hat{1}_j \hat{a}_{j+1}^2] = -2\sqrt{2}|1_j 0_{j+1}\rangle\langle 2_j 1_{j+1}|. \quad (\text{S95})$$

After straightforward calculations, we obtain

$$[\hat{H}_{\text{corr},1}, \hat{J}^+] = -4J_{\text{corr},1} \sum_j (-1)^j \hat{h}_{j,j+1}, \quad (\text{S96})$$

$$[\hat{H}_{\text{corr},2}, \hat{J}^+] = -2J_{\text{corr},2} \sum_j (-1)^j \hat{h}_{j,j+1}. \quad (\text{S97})$$

This result suggests that

$$[\hat{H}_0, \hat{J}^+] \propto [\hat{H}_{\text{corr},1}, \hat{J}^+] \propto [\hat{H}_{\text{corr},2}, \hat{J}^+]. \quad (\text{S98})$$

As in the case of the Hamiltonian \hat{H}_0 , because both commutation relations contain the term $\sum_j (-1)^j \hat{h}_{j,j+1}$ with $\hat{h}_{j,j+1}|\psi_0\rangle = 0$, we have

$$[\hat{H}_{\text{corr},1}, \hat{J}^+]|\psi_0\rangle = 0, \quad (\text{S99})$$

$$[\hat{H}_{\text{corr},2}, \hat{J}^+]|\psi_0\rangle = 0. \quad (\text{S100})$$

It is also clear that

$$[[\hat{H}_{\text{corr},1}, \hat{J}^+], \hat{J}^+] = 0, \quad (\text{S101})$$

$$[[\hat{H}_{\text{corr},2}, \hat{J}^+], \hat{J}^+] = 0. \quad (\text{S102})$$

Thus, the Hamiltonian $\hat{H} + \hat{H}_{\text{corr},1} + \hat{H}_{\text{corr},2}$ satisfies the RSGA-1. The QMBS states for the Hamiltonian \hat{H} are also those for the Hamiltonian $\hat{H} + \hat{H}_{\text{corr},1} + \hat{H}_{\text{corr},2}$.

D. Without the three-body constraint

From the viewpoint of the RSGA, we can understand how the present QMBS states break down without the three-body constraint. For soft-core bosons, we obtain

$$\begin{aligned}
\hat{H}|22 \cdots 22\rangle &= -J \sum_j (\hat{b}_{j+1}^\dagger \hat{b}_j + \hat{b}_j^\dagger \hat{b}_{j+1})|22 \cdots 22\rangle \\
& + LU|22 \cdots 22\rangle \quad (\text{S103})
\end{aligned}$$

$$\begin{aligned}
&= -\sqrt{6}J \sum_j (| \underbrace{22 \cdots 22}_{j-1} 13 \underbrace{22 \cdots 22}_{L-j-1} \rangle \\
& + | \underbrace{22 \cdots 22}_{j-1} 31 \underbrace{22 \cdots 22}_{L-j-1} \rangle) \\
& + LU|22 \cdots 22\rangle, \quad (\text{S104})
\end{aligned}$$

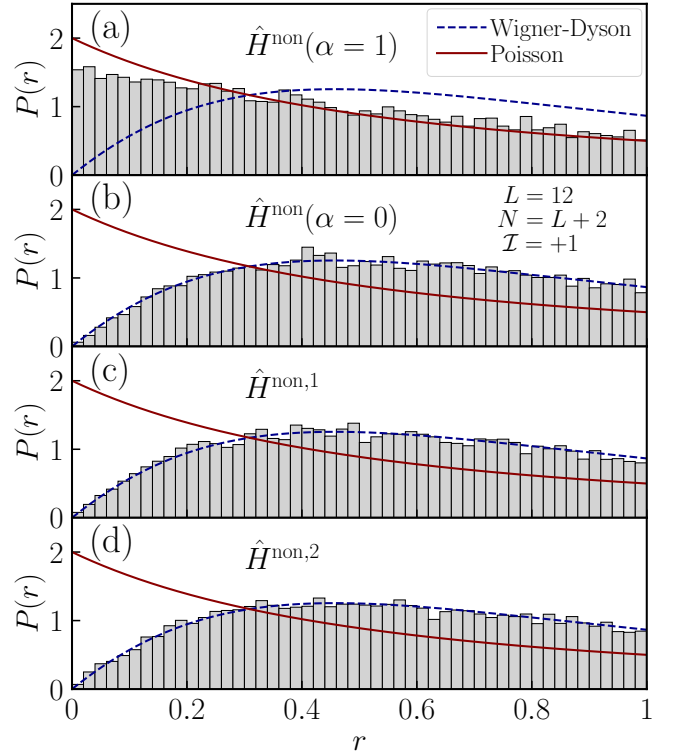


FIG. S1. Distribution $P(r)$ of the level spacing ratio. The models (a) $\hat{H}^{\text{non}}(\alpha = 1)$, (b) $\hat{H}^{\text{non}}(\alpha = 0)$, (c) $\hat{H}^{\text{non},1}$, and (d) $\hat{H}^{\text{non},2}$ for $L = 12$ are chosen [see Eqs. (S105)–(S107)]. We focus on the particle number $N = L + 2$ in the even parity sector ($\mathcal{I} = +1$) under open boundary conditions. As for $\hat{H}^{\text{non}}(\alpha = 1)$, $P(r)$ almost agrees with that of the Poisson distribution, suggesting that the model is integrable-like. For the other models, $P(r)$ exhibits the Wigner-Dyson distribution, meaning that the model is nonintegrable.

which means that the state $|\psi_0\rangle = |22 \cdots 22\rangle$ is no longer the eigenstate of the Hamiltonian. Therefore, the Hamiltonian does not satisfy the RSGA. Note that, although the present QMBS states do not survive without the three-body constraint, the existence of other types of QMBS states is not ruled out in general.

S-IV. NUMERICAL RESULTS

A. Nonintegrability of each model

Before we confirm the presence of the QMBS states in the relevant Bose-Hubbard-like models numerically, let us examine the nonintegrability of these models. The Bose-Hubbard model for $U \neq 0$ and $J \neq 0$ is nonintegrable [S15], and that at $U = 0$ (the free boson model) or $J = 0$ (the atomic limit) is integrable. On the other hand, additional constraints often work as effective interactions even in the absence of explicit interaction terms. It is less trivial whether the Bose-Hubbard model with a three-body constraint or that with correlated hopping terms is nonintegrable. We will demonstrate that, for $J \neq 0$, such models at $U = 0$ are nonintegrable in most cases, whereas

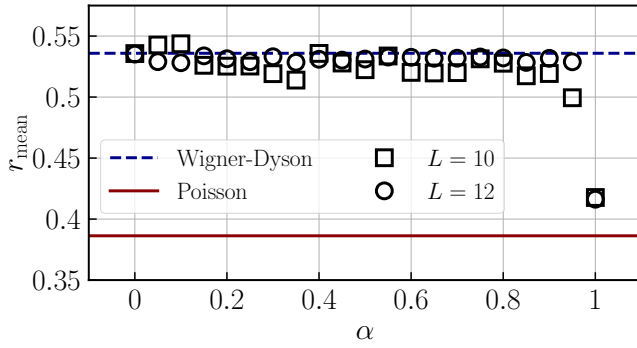


FIG. S2. Mean level spacing ratio r_{mean} as a function of α for the model $\hat{H}^{\text{non}}(\alpha)$ defined in Eq. (S105). Squares and circles correspond to those obtained for $L = 10$ and $L = 12$, respectively. We consider the particle number $N = L + 2$ in the even parity sector ($\mathcal{I} = +1$) under open boundary conditions. The model becomes the Bose-Hubbard model without any correlated hoppings at $\alpha = 0$, whereas it is equivalent to the $S = 1$ XY model at $\alpha = 1$. For $\alpha < 1$, r_{mean} is close to the value expected in the Wigner-Dyson distribution, indicating that the model is nonintegrable in this parameter region.

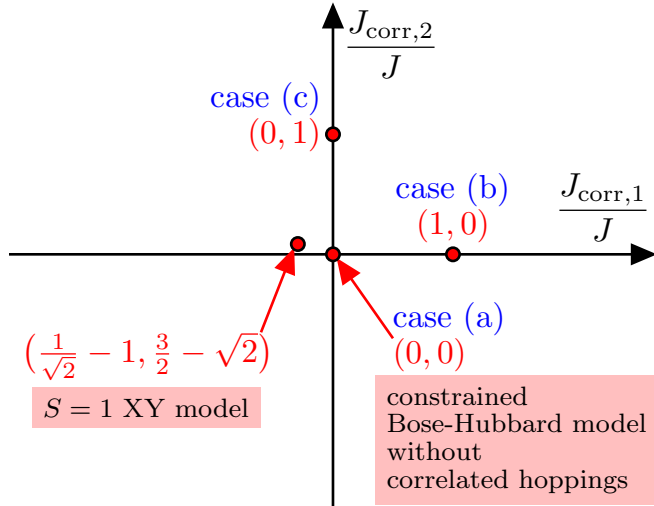


FIG. S3. Parameter points that we have chosen to study the energy dependence of the EE. See Fig. S4 for the numerical results.

the model at $U = 0$ accidentally becomes integrable-like only when it is exactly mapped to the $S = 1$ XY model.

We focus on the following (noninteracting) Bose-Hubbard model with the correlated hopping terms under a three-body constraint

$$\hat{H}^{\text{non}}(\alpha) = \hat{H}_0 + \hat{H}_{\text{corr},1} \left[J_{\text{corr},1} = \left(\frac{1}{\sqrt{2}} - 1 \right) \alpha J \right] + \hat{H}_{\text{corr},2} \left[J_{\text{corr},2} = \left(\frac{3}{2} - \sqrt{2} \right) \alpha J \right], \quad (\text{S105})$$

where \hat{H}_0 , $\hat{H}_{\text{corr},1}$, and $\hat{H}_{\text{corr},2}$ are defined in Eqs. (S3), (S36), and (S37), respectively. When $\alpha = 0$, the model reduces to the Bose-Hubbard model without the correlated hoppings. On the other hand, when $\alpha = 1$, the model is equivalent to the

$S = 1$ XY model. The $S = 1$ XY model is known to exhibit integrable-like behavior in the even total magnetization sector because of a twisted SU(2) symmetry in open and artificial boundary conditions [S1, S4, S12]. (In the sector where the total spin is maximum, the Hamiltonian becomes a constant matrix and the system trivially exhibits integrable behavior.) As we will see below, we have examined the nonintegrability of these models for $\alpha = 0, 0.05, 0.1, \dots, 0.95, 1$ and found that the only $\alpha = 1$ point is singular.

In addition, we specifically consider the following models with each correlated hopping term

$$\hat{H}^{\text{non},1} = \hat{H}_0 + \hat{H}_{\text{corr},1}(J_{\text{corr},1} = J), \quad (\text{S106})$$

$$\hat{H}^{\text{non},2} = \hat{H}_0 + \hat{H}_{\text{corr},2}(J_{\text{corr},2} = J). \quad (\text{S107})$$

As we will show below, these models are found to be nonintegrable as well. We will also demonstrate how the QMBS states appear for these models by looking into their EE in the next section.

We investigate the nonintegrability of the models by looking at the distribution $P(r)$ of the level spacing ratio, which is defined as

$$r_n = \frac{\min(s_n, s_{n+1})}{\max(s_n, s_{n+1})} \in [0, 1], \quad (\text{S108})$$

$$s_n = \frac{E_{n+1} - E_n}{J} \quad (\text{S109})$$

with $\{E_n\}$ being the ordered list of eigenenergies [S16–S19]. The model is inferred to be integrable-like (nonintegrable) when $P(r)$ obeys the Poisson distribution $P(r) = 2/(1+r)^2$ [the Wigner-Dyson distribution $P(r) = (r+r^2)^\beta/(1+r+r^2)^{1+3\beta/2}/Z_\beta$ with β being the Dyson index equal to 1 and $Z_{\beta=1} = 4/27$ for the Gaussian orthogonal ensemble] [S19]. We also calculate the mean level spacing ratio, which is given as

$$r_{\text{mean}} = \langle r_n \rangle. \quad (\text{S110})$$

Here, the symbol $\langle \dots \rangle$ represents the average over all states in the given symmetric sector. We compare the estimated mean level spacing ratio with the expected $r_{\text{mean}} = 4 - 2\sqrt{3} \approx 0.536$ (Wigner-Dyson distribution) or $r_{\text{mean}} = 2 \ln 2 - 1 \approx 0.386$ (Poisson distribution) [S18] to determine whether the model is likely to be nonintegrable.

To this end, we calculate all the eigenenergies for a certain symmetry sector of the models by the exact diagonalization method. To carefully capture the possible integrable-like behavior in the energy spectrum, we choose the even total number sector, corresponding to the even total magnetization sector in the $S = 1$ XY model. Hereafter, we display the results for the particle number $N = L + 2$ in the even parity sector ($\mathcal{I} = +1$) under open boundary conditions. The system size is chosen to be $L = 10$ and $L = 12$, whose dimensions of the Hilbert spaces are 3405 and 29202, respectively.

We show the distribution $P(r)$ at $L = 12$ for the models $\hat{H}^{\text{non}}(\alpha = 1)$, $\hat{H}^{\text{non}}(\alpha = 0)$, $\hat{H}^{\text{non},1}$, and $\hat{H}^{\text{non},2}$ in Fig. S1. In the case of $\hat{H}^{\text{non}}(\alpha = 1)$, which also corresponds to the $S = 1$ XY model having the integrable-like behavior in even magnetic

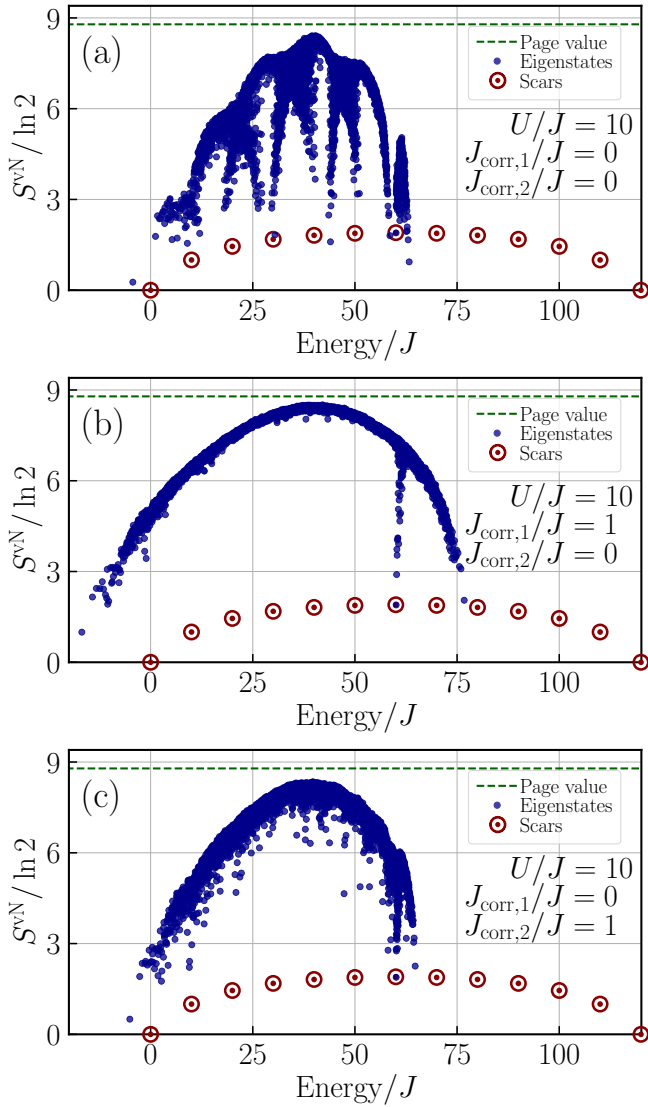


FIG. S4. EE as a function of energy in the presence of correlated hoppings. We consider the system size $L = 12$ under open boundary conditions and the interaction strength $U/J = 10$ in Eq. (S35). The correlated hopping is chosen as (a) $(J_{\text{corr},1}/J, J_{\text{corr},2}/J) = (0, 0)$, (b) $(J_{\text{corr},1}/J, J_{\text{corr},2}/J) = (1, 0)$, and (c) $(J_{\text{corr},1}/J, J_{\text{corr},2}/J) = (0, 1)$ [see Fig. S3]. The quantum number sector with the particle number $N = L$ (unit filling) and the even parity $\mathcal{I} = +1$ is given by blue dots. The largest EE almost saturates at the Page value [S20] $S^{\text{Page}} = (\ln 3)L/2 - 1/2$ [S1, S4] (a green dashed line). Each QMBS state (a red circle with a dot) with the particle number N has the energy $UN/2$ and the expectation values $\langle \sum_{i=1}^L \hat{n}_i \rangle = N$ and $\langle \sum_{i=1}^L \hat{n}_i^2 \rangle = 2N$. Its half-chain EE at $N = L$, corresponding to a state $|S_{n=L/2}\rangle$, becomes $S_A^{vN} \rightarrow [\ln(\pi L/8) + 1]/2$ for $L \rightarrow \infty$. Irrespective of the choice of the correlated hopping parameters $J_{\text{corr},1}$ and $J_{\text{corr},2}$, each QMBS state has the same energy and the same EE.

sectors, $P(r)$ almost obeys the Poisson distribution. The small deviation from the expected Poisson distribution may be due to the presence of unresolved symmetries in even total number sectors [S4]. Therefore, it is plausible that the model $\hat{H}^{\text{non}}(\alpha = 1)$ is integrable-like. On the other hand, $P(r)$'s of the other

models obey the Wigner-Dyson distribution, suggesting that these systems are nonintegrable.

We also calculate the mean level spacing ratio r_{mean} for the model $\hat{H}^{\text{non}}(\alpha)$ in Fig. S2. At $\alpha = 1$, the model is equivalent to the $S = 1$ XY model. As we expected, the integrable-like behavior also appears in the mean level spacing, and r_{mean} takes the value close to that of the Poisson distribution ($r_{\text{mean}} \approx 0.386$). On the other hand, for $\alpha < 1$, r_{mean} is nearly equal to that of the Wigner-Dyson distribution ($r_{\text{mean}} \approx 0.536$). These results indicate that $\hat{H}^{\text{non}}(\alpha)$ is nonintegrable except for the special point $\alpha = 1$.

B. Bipartite EE

We numerically confirm the existence of the QMBS states satisfying the relations predicted in Sec. S-I A. On some of the points that we have chosen [see Fig. S3], we show the energy dependence of the EE for the Hamiltonian in Eq. (S35) with $V = \mu = 0$ [see Fig. S4 and Fig. 1 in the main text]. All the eigenstates in the even number of total particles ($N = 0, 2, 4, \dots, 2L - 2, 2L$) are calculated for the model with the open boundary condition by the exact diagonalization method using the QuSpin library [S21, S22]. In particular, we calculate the even parity $\mathcal{I} = +1$ (odd parity $\mathcal{I} = -1$) sector when $N = 4m$ ($N = 4m + 2$) with m being an integer. The EE is obtained from the singular value decomposition of a wave function utilizing $U(1)$ symmetry [S23], associated with the conservation of the total particle number [S24–S27]. We specifically display all the eigenstates with $N = L$ and the QMBS states for $N = 0, 2, 4, \dots, 2L - 2, 2L$.

For a weaker interaction ($U/J = 1$) in the case of the Hamiltonian H in Eq. (S2), the data points for different N distribute similarly [see Fig. 1 in the main text]. In each sector N , the QMBS state with the energy $UN/2$ exhibits the area-law EE with a logarithmic correction. On the other hand, for a stronger interaction ($U/J = 10$) [see Fig. S4(a)], we observe a more separated structure (EE peaks around the energy $\approx 10J, 20J, 30J$, and $40J$) in the energy spectra than in the case of $U/J = 1$. Even in this case, we still confirm the presence of the QMBS states.

We also numerically examine the effect of the correlated hopping terms. We calculate all eigenstates of the generalized Bose-Hubbard model in Eq. (S35) with $V = \mu = 0$. We consider the system with $L = 12$ at $U/J = 10$ as in the case of Fig. S4(a). We choose only the correlated hopping $J_{\text{corr},1}/J = 1$ in Fig. S4(b), whereas only $J_{\text{corr},2}/J = 1$ in Fig. S4(c), in addition to the conventional hopping J . They are nonintegrable as we have confirmed in Sec. S-IV A. These spectra are less separated than in the case of Fig. S4(a) because the additional correlated hopping terms weaken the effect of interaction. The athermal eigenstates still remain in the presence of the correlated hopping term and have exactly the same energy as that without the correlated hoppings.

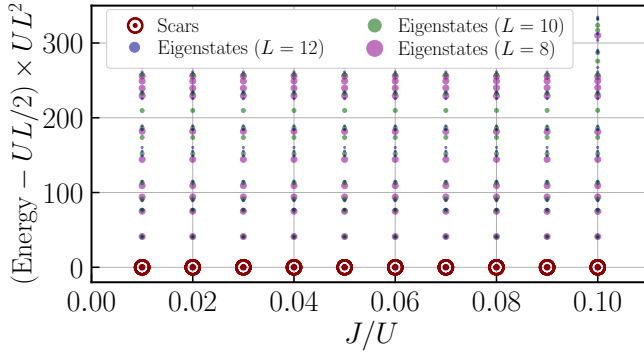


FIG. S5. Magnified energy spectra as a function of the interaction strength at unit filling. The parameters are the same as in Fig. 2 of the main text.

C. Size dependence of the energy spectra

We check the finite-size effect of the energy spectra in the strong-coupling limit. We focus on the system sizes up to $L = 12$. At unit filling for the symmetry sector where the QMBS state exists, the dimension of the Hilbert space is 563 for $L = 8$, 4451 for $L = 10$, and 36965 for $L = 12$.

We multiply the energy by UL^2 to inspect the excitations clearly, as shown in Fig. S5. In the strong-coupling limit, the lower excitations are essentially characterized by those of the ferromagnetic Heisenberg model with the spin exchange interaction, which is proportional to J^2/U (see the main text). Since the excitation of the ferromagnetic Heisenberg model on a lattice grows as k^2 for momenta $k = 2n\pi/L$ with a small integer number n , we expect that the lowest excitation in a finite system scales as $1/(UL^2)$ in the unit of J . This behavior is correctly observed, and the scaled lowest excitations show very small size and interaction dependencies for $L \geq 8$ and $J/U \leq 0.1$.

D. Effect of external potential

We examine the half-chain entanglement entropy in the presence of the parabolic potential. We consider the Hamiltonian

$$\hat{H} = -J \sum_{i=1}^{L-1} (\hat{a}_i^\dagger \hat{a}_{i+1} + \hat{a}_{i+1}^\dagger \hat{a}_i) + \sum_{i=1}^L \Omega_i \hat{n}_i + \frac{U}{2} \sum_{i=1}^L \hat{n}_i (\hat{n}_i - 1) \quad (\text{S111})$$

and choose the external potential $\Omega_i = \Omega[i - (L+1)/2]^2$, where $\Omega > 0$ is the strength of the potential. In the absence of the potential ($\Omega = 0$), at each filling ($\langle \sum_{i=1}^L \hat{n}_i \rangle = N$), we numerically find that the QMBS state satisfies $\langle \sum_{i=1}^L \hat{n}_i^2 \rangle = 2N$, whereas other eigenstates are found to exhibit $\langle \sum_{i=1}^L \hat{n}_i^2 \rangle < 2N$. This observation suggests that, in each particle number sector, the eigenstate having the largest $\langle \sum_{i=1}^L \hat{n}_i^2 \rangle$ corresponds to the QMBS state. In the presence of small potential ($0 < \Omega \ll J$), we anticipate this trend to continue and can safely regard the eigenstate with the largest $\langle \sum_{i=1}^L \hat{n}_i^2 \rangle$ as the remnant of the

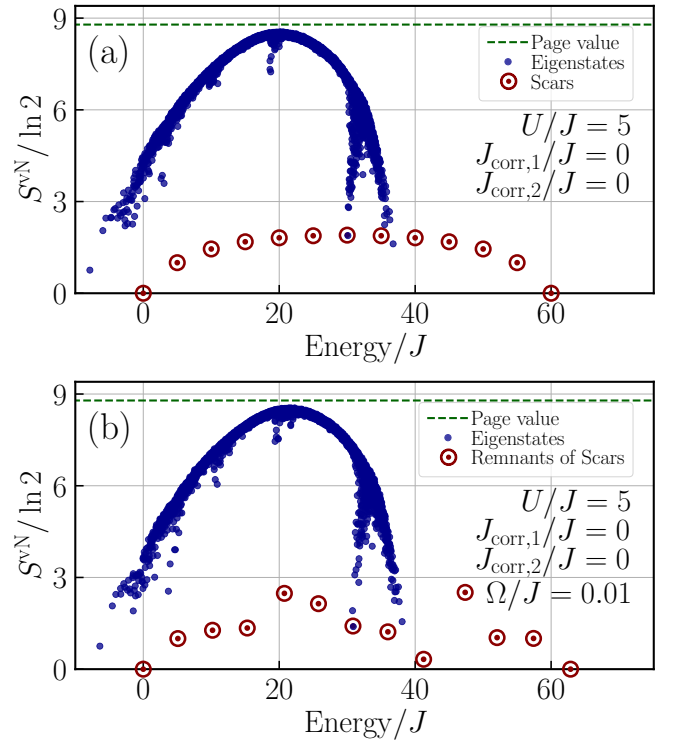


FIG. S6. Entanglement entropy as a function of energy for (a) without external potential and (b) with external potential. We consider the system size $L = 12$ under open boundary conditions and the interaction strength $U/J = 5$ in Eq. (S35). Remnants of scars are characterized by the largest $\langle \sum_{i=1}^L \hat{n}_i^2 \rangle (\approx 2N)$ in each sector of particle number $\langle \sum_{i=1}^L \hat{n}_i \rangle = N$.

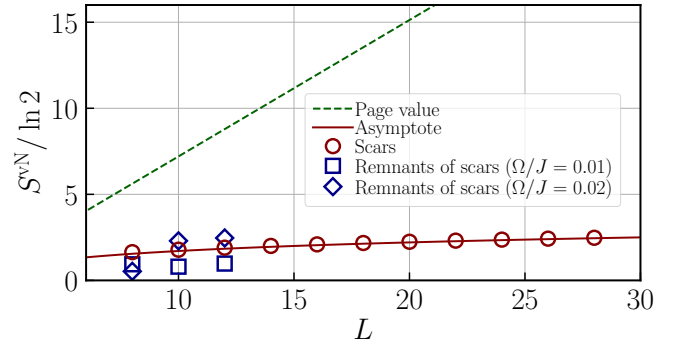


FIG. S7. Size dependence of entanglement entropy of scars with and without external potential. The entanglement entropy grows in a similar manner regardless of the presence or absence of the external potential.

QMBS state. Indeed, such state still exhibits a very small entanglement entropy. As shown in Fig. S6, in the presence of a small external potential ($\Omega/J = 0.01$), we find that remnants of the QMBS states exhibit entanglement entropies much smaller than those for volume-law states.

We also investigate the size dependence of the half-chain entanglement entropy at unit filling in the presence of the

parabolic potential (see Fig. S7). The exact QMBS state without the potential shows the entanglement entropy $S_A^{\text{vN}} = -\sum_{k=0}^{L/2} \lambda_k \ln \lambda_k$ with $\lambda_k = \binom{L/2}{k} \binom{L/2}{L/2-k} / \binom{L}{L/2}$, which nearly grows as $S_A^{\text{vN}} \approx [\ln(\pi L/8) + 1]/2$ for a sufficiently large size L [S1]. This value is much smaller than the Page value [S20] $S^{\text{Page}} = (\ln 3)L/2 - 1/2$ [S1, S4]. In a similar manner, in the presence of the external potential ($\Omega/J = 0.01, 0.02$), the remnants of the QMBS states show the entanglement entropy close to the one with the QMBS state without the potential.

Within the sizes that we could study, they seem to be consistent with the logarithmic size dependence of the entanglement entropy growth. The presence of small external potential does not affect the QMBS states significantly.

Note that the Bose-Hubbard simulator in a flat box potential has been realized very recently [S28, S29]. Therefore, one may prepare the ideal QMBS states without any potential effects experimentally.

-
- [S1] M. Schechter and T. Iadecola, *Phys. Rev. Lett.* **123**, 147201 (2019).
- [S2] S. Moudgalya, N. Regnault, and B. A. Bernevig, *Phys. Rev. B* **102**, 085140 (2020).
- [S3] M. Kunimi and I. Danshita, *Phys. Rev. A* **104**, 043322 (2021).
- [S4] S. Chattopadhyay, H. Pichler, M. D. Lukin, and W. W. Ho, *Phys. Rev. B* **101**, 174308 (2020).
- [S5] C. C. Gerry, *J. Opt. Soc. Am. B* **8**, 685 (1991).
- [S6] C. C. Gerry, *J. Opt. Soc. Am. B* **8**, 1999 (1991).
- [S7] P.-A. Lindgard and O. Danielsen, *J. Phys. C: Solid State Phys.* **7**, 1523 (1974).
- [S8] E. G. Batyev, *Zh. Eksp. Teor. Fiz.* **89**, 308 (1985).
- [S9] G. Marmorini, D. Yamamoto, and I. Danshita, *Phys. Rev. B* **93**, 224402 (2016).
- [S10] M. Vogl, P. Laurell, H. Zhang, S. Okamoto, and G. A. Fiete, *Phys. Rev. Res.* **2**, 043243 (2020).
- [S11] J. König and A. Hucht, *SciPost Phys.* **10**, 7 (2021).
- [S12] A. Kitazawa, K. Hijii, and K. Nomura, *J. Phys. A: Math. Gen.* **36**, L351 (2003).
- [S13] H. Zhao, J. Vovrosh, F. Mintert, and J. Knolle, *Phys. Rev. Lett.* **124**, 160604 (2020).
- [S14] A. Hudomal, I. Vasić, N. Regnault, and Z. Papić, *Commun. Phys.* **3**, 99 (2020).
- [S15] A. R. Kolovsky and A. Buchleitner, *Europhys. Lett.* **68**, 632 (2004).
- [S16] V. Oganesyan and D. A. Huse, *Phys. Rev. B* **75**, 155111 (2007).
- [S17] A. Pal and D. A. Huse, *Phys. Rev. B* **82**, 174411 (2010).
- [S18] Y. Y. Atas, E. Bogomolny, O. Giraud, and G. Roux, *Phys. Rev. Lett.* **110**, 084101 (2013).
- [S19] W. W. Ho and Đ. Radičević, *Int. J. Mod. Phys. A* **33**, 1830004 (2018).
- [S20] D. N. Page, *Phys. Rev. Lett.* **71**, 1291 (1993).
- [S21] P. Weinberg and M. Bukov, *SciPost Phys.* **2**, 003 (2017).
- [S22] P. Weinberg and M. Bukov, *SciPost Phys.* **7**, 020 (2019).
- [S23] J.-H. Jung and J. D. Noh, *J. Korean Phys. Soc.* **76**, 670 (2020).
- [S24] J. Schnack, P. Hage, and H.-J. Schmidt, *J. Comput. Phys.* **227**, 4512 (2008).
- [S25] J. Zhang and R. Dong, *Eur. J. Phys.* **31**, 591 (2010).
- [S26] A. Szabados, P. Jeszszski, and P. R. Surján, *Chem. Phys.* **401**, 208 (2012).
- [S27] D. Raventós, T. Graß, M. Lewenstein, and B. Juliá-Díaz, *J. Phys. B: At., Mol. Opt. Phys.* **50**, 113001 (2017).
- [S28] A. Impertro, J. F. Wienand, S. Häfele, H. von Raven, S. Hubele, T. Klostermann, C. R. Cabrera, I. Bloch, and M. Aidelsburger, *Commun. Phys.* **6**, 166 (2023).
- [S29] J. F. Wienand, S. Karch, A. Impertro, C. Schweizer, E. McCulloch, R. Vasseur, S. Gopalakrishnan, M. Aidelsburger, and I. Bloch, *arXiv:2306.11457*.